REVIEW

Nickel sulfide-based energy storage materials for high-performance electrochemical capacitors

Ramyakrishna Pothu, Ravi Bolagam, Qing-Hong Wang*, Wei Ni* [iD] **,
Jin-Feng Cai, Xiao-Xin Peng, Yue-Zhan Feng, Jian-Min Ma*** [iD]

Abstract Supercapacitors are favorable energy storage devices in the field of emerging energy technologies with high power density, excellent cycle stability and environmental benignity. The performance of supercapacitors is definitively influenced by the electrode materials. Nickel sulfides have attracted extensive interest in recent years due to their specific merits for supercapacitor application. However, the distribution of electrochemically active sites critically limits their electrochemical performance. Notable improvements have been achieved through various strategies such as building synergetic structures with conductive substrates, enhancing the active sites by nanocrystallization and constructing nanohybrid architecture with other electrode materials. This article overviews the progress in the reasonable design and preparation of nickel sulfides and their composite electrodes combined with various bifunctional electric double-layer capacitor (EDLC)-based substances (e.g., graphene, hollow carbon) and pseudocapacitive materials (e.g., transition-metal oxides, sulfides, nitrides). Moreover, the corresponding electrochemical performances, reaction mechanisms, emerging challenges and future perspectives are briefly discussed and summarized.

Keywords Supercapacitors; Nickel sulfides; Hybrid structures; Energy storage materials; Pseudocapacitance

R. Pothu, R. Bolagam, J.-M. Ma*
School of Physics and Electronics, Hunan University, Changsha 410082, China
e-mail: nanoelechem@hnu.edu.cn

Q.-H. Wang*
School of Chemistry and Materials Science, Jiangsu Key Laboratory of Green Synthetic Chemistry for Functional Materials, Jiangsu Normal University, Xuzhou 221116, China
e-mail: wangqh@jsnu.edu.cn

W. Ni
Institute for Advanced Study, Chengdu University, Chengdu 610106, China

W. Ni*
Faculty of Technology, University of Oulu, Oulu 90014, Finland
e-mail: niwei@iccas.ac.cn

J.-F. Cai, X.-X. Peng
Yiyang Wanjingyuan Electronics Co., Ltd., Yiyang 413000, China

Y.-Z. Feng
Key Laboratory of Materials Processing and Mold (Zhengzhou University), Ministry of Education, Zhengzhou University, Zhengzhou 450002, China

1 Introduction

In recent years, energy storage and conversion have drawn a great deal of attention due to the employment of various sustainable energy technologies [1–6]. A lot of technologies have been developed, such as lithium–air batteries (LABs) [5, 6], lithium–sulfide batteries (LSBs) [7–11], lithium-ion batteries (LIBs) [12–16], sodium-ion batteries (SIBs) [17–23], potassium-ion batteries (PIBs) [24–28], zinc-ion batteries [29, 30], zinc–air batteries [31, 32] and supercapacitors (SCs) [33–36]. Among them, SCs (also named electrochemical capacitors, ECs) have great potential to fulfill the challenges for energy storage and conversion due to the fast charging and discharging, more power density, good cycle stability, besides relatively low cost [37–43]. The superior high power density makes SCs a promising electrochemical device for high-power harvesting applications featuring ultralong life span [44–46]. It is known that the capacitance characteristics of SCs are

influenced by electrodes, electrolytes and assembly techniques, the most important of which is the electrode materials. Accordingly, it is extremely important to introduce capable electrode substances with the highest specific capacitance, magnificent power density to meet superior cycle stability [47–49].

Depending on the energy storage mechanism, SCs can be categorized into two types: electric double-layer capacitors (EDLCs) and pseudocapacitors (PCs). EDLCs energy storage is built upon an electric double-layer effect, occurring at the electrode–electrolyte interaction achieved through transferring the electron charge between electrolyte and electrode via adsorption/desorption and ion transfer in electrochemical reactions [48–50]. PCs are based on an electrochemical storage mechanism by virtue of reversible Faradaic redox reaction on/near the electrode surface. Compared with EDLCs, PCs usually show higher specific capacitance and higher energy density [50, 51]. The specific capacitance of PCs depends mainly on the surface area of active materials and the structure of electrodes [52–54]. Transition-metal oxide/hydroxides/sulfides [55–60] and conducting polymers [41, 61] are broadly investigated as pseudocapacitive electrode materials. Transition-metal oxides/hydroxides deliver high energy density but are hampered by their low rate capability. Conducting polymers show high specific capacitance, yet suffer from poor cycle stability [62–65]. Transition-metal sulfides are proved to be one of the most potential electrode materials for SCs [66–69]. Based on their favorable Faradaic redox reaction, metal sulfides, such as NiS_x, CoS_x, FeS_x, MnS_x, CuS_x and MoS_2, are the desired choice [70–75]. Group of nickel sulfides (Ni_xS_y) is comprised of Ni and S with various stoichiometric proportions, including NiS, NiS_2, Ni_3S_2, Ni_3S_4, Ni_6S_5, Ni_7S_6 and Ni_9S_8 due to the low electronegativity of sulfur easily constructed with nickel. Due to the rich chemical composition, natural abundance, large capacitance and high conductivity as well as environmental benignity, nickel sulfides have been widely used in SCs [76–78]. In particular, their vital specific capacitance (several times higher than that of carbon/graphite-attribute substances) makes them stand out from other electrode materials [79, 80]. These merits of nickel sulfides drive their rapid development for SCs. There are various reviews on metal sulfides for energy storage and conversion [58, 59, 70, 71]; however, there is no systematic review on nickel sulfides for SCs. Therefore, it is necessary and timely to review the latest advances in nickel sulfides. This review summarizes the synthesis methods, the morphology/composite-dependent electrochemical properties, challenges and perspectives of various nickel sulfides for SCs.
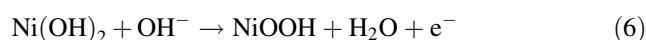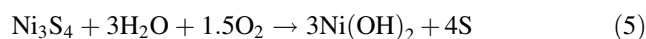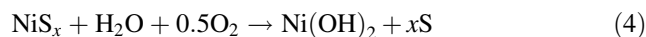
2 Reaction mechanism

The redox reactions of nickel sulfides in alkaline electrolytes are generally as follows [81]:

$$NiS_x + OH^- \leftrightarrow NiS_xOH + e^- \tag{1}$$

$$Ni_3S_2 + 3OH^- \leftrightarrow Ni_3S_2(OH)_3 + 3e^- \tag{2}$$
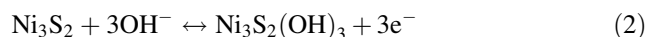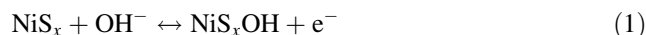
Semi-infinite diffusion-limited reaction process verifies the electrochemical responses of active electrode materials to differentiate the redox mechanism of battery (value of the exponent, $b = 0.5$) or PCs-type electrodes, for the kinetic process of the electrode and redox reaction is controlled by a semidefinite diffusion. The peak current (I) versus scan rate (v) at a constant voltage window in cyclic voltammograms (CV) can be acknowledged and described as follows (a and b are adjustable parameters) [48]:

$$I = av^b \tag{3}$$

However, the poor cycling execution of Ni_xS_y could usually be accompanied by irreversible reactions:

$$NiS_x + H_2O + 0.5O_2 \rightarrow Ni(OH)_2 + xS \tag{4}$$

$$Ni_3S_4 + 3H_2O + 1.5O_2 \rightarrow 3Ni(OH)_2 + 4S \tag{5}$$

$$Ni(OH)_2 + OH^- \rightarrow NiOOH + H_2O + e^- \tag{6}$$

According to previous reports [81–83], the battery-type redox mechanism of Ni_xS_y electrodes and the lower rate performance and poor cycling stability thereof will significantly hamper their extensive applications. The main drawback of nickel sulfides is their fast-decayed capacitance at high rates (viz. relatively low cycle stability), which results from their low intrinsic electrical conductivity and inadequate amount of electroactive sites. The proposed strategies to overcome the abovementioned problems include designed synthesis of nanostructures, binder-free electrodes grown on conductive substrates [84–87] and fabrication of nanohybrids with good conductive supports such as porous carbons [88–91], graphene [92–95] and conducting polymers [96–101]. It is well known that the electrochemical performances largely depend on the morphology and surface area of electrode materials; thus, the controlled synthesis of nickel sulfide nanomaterials with stable structure and large surface area is of great importance [102–105].

3 NiS

3.1 Pristine NiS

Among the various Ni_xS_y compositions, NiS possesses the best easiest stoichiometry occurring in two possible phases

of α-NiS (hexagonal, *P63/mmc*) and β-NiS (rhombohedral, *R3m*). NiS is extremely beneficial owing to its huge theoretical capacity (1060 F·g^{-1}) [106, 107], good electrical conductivity, low cost, easy fabrication process and environmental sustainability. Hou et al. [108] firstly used NiS as electrode material for SCs and revealed the main drawback to be the low rate capability, which arises from the poor electrical conductivity and limited electron transport rate. An effective method to resolve the above-mentioned problems is to construct diverse nanostructured NiS with different dimensions, including nanorods [109], nanoplates [110], nanowires [111], porous nanomaterials, etc., as well as hierarchical architectures including core–shell, complex hollow structures via various synthesis methods such as hydrothermal method, anion exchange reaction and potentiodynamic deposition.

As electrode materials, hollow nanostructures possess the advantages of huge electrolyte accessible surface area and abundant electroactive sites. For example, Chen et al. [112] designed a facile template-engaged route to prepare nickel sulfides besides copper sulfide hierarchical hollow spheres. The NiS hollow structure (Fig. 1a) exhibits high BET specific surface area of 124 m^2·g^{-1} with a standard pore size of 3.5 nm (Fig. 1b) and delivers great specific capacitances of 1460 and 727 F·g^{-1} at current densities of

4 and 20 A·g^{-1}, respectively (Fig. 1c), as well as excellent capacitance retention (93.6% after 5000 charge–discharge cycles at 12 A·g^{-1}) (Fig. 1d). Considering the advantages of hollow structure, Wang et al. [113] developed NiS hierarchical hollow microspheres through a template-free sulfidation process using α-Ni(OH)$_2$ microspheres as precursor. The unique hierarchical hollow spherical structure can provide more electroactive sites and efficiently smooth the contact between the active materials and electrolyte. The as-synthesized NiS exhibited a high specific capacity of 153.6 mAh·g^{-1} at a current density of 0.5 A·g^{-1} at high mass loading, which can be attributed to its small crystal size, hierarchically porous structure and high electrical conductivity.

The construction of hierarchical structures will guarantee the electrode stability compared to that of discrete/isolated nanostructures for enhanced performance. For example, the heterogeneous reactions at the substrate surface can cause nucleation, aggregation and coalescence, as well as the growth of thin film [114]. The unique β-NiS thin films with different morphologies of nanoneedles, nanoplates and nanoflowers are fabricated by Patil et al. [114] via a hydrothermal process with Ni(OH)$_2$ thin films as precursors on stainless strip substrate. Among these nanostructures, stacked nanoneedle morphology of β-NiS

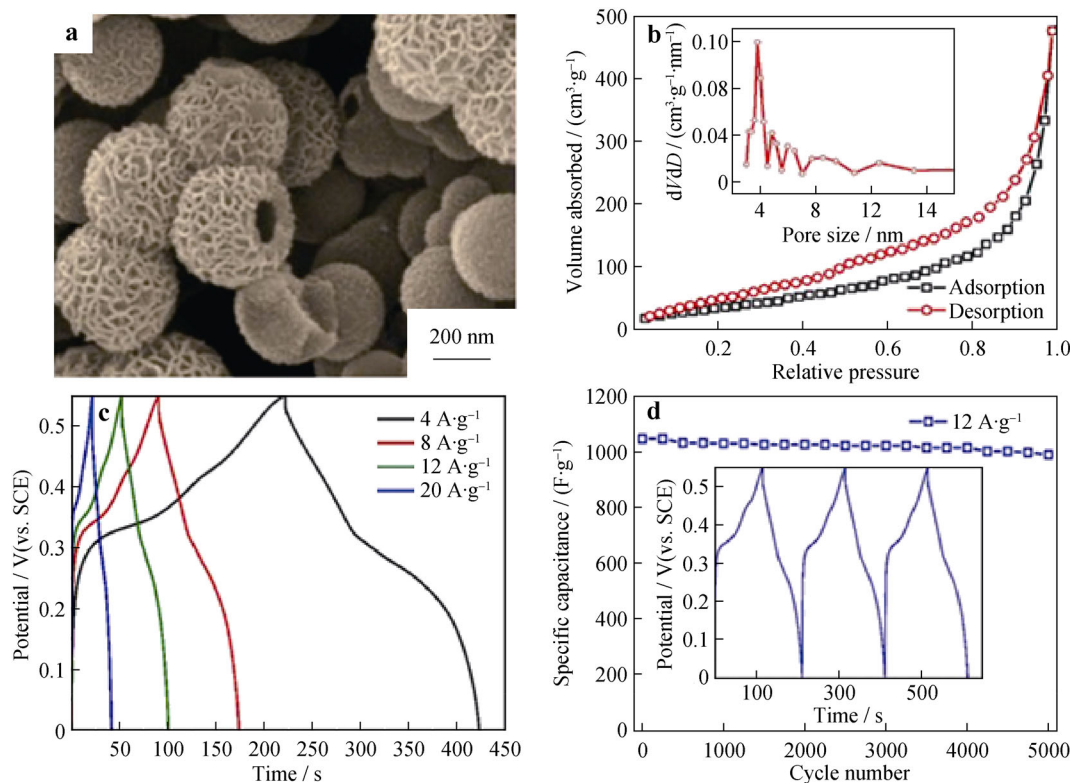**Fig. 1** Structural characterization and electrochemical performance of NiS hollow nanostructure: **a** SEM image; **b** nitrogen adsorption–desorption isotherm (inset being distribution of pore size); **c** GCD curves at different current densities; **d** cycling performance at 12 A·g^{-1} (inset being first three charge–discharge curves). (reproduced from Ref. [112], Copyright 2017 Springer Nature)

thin film exhibits the highest specific capacitance of 416 $F \cdot g^{-1}$ at 0.5 $mA \cdot cm^{-2}$. This superior performance was credited with its open porous structure that offers huge electroactive surface area and straightforward path for insertion/de-insertion of electrolyte ions within the active electrode. Furthermore, the flexible solid-state symmetric supercapacitors (FSS-SCs) assembled with β-NiS thin films and polyvinyl alcohol–lithium perchlorate (PVA–LiClO$_4$) as a polymer gel electrolyte exhibit a capacitance of 55.8 $F \cdot g^{-1}$ with a scan rate of 10 $mV \cdot s^{-1}$ at potential window of 1.2 V, as well as good cycle stability. Yu et al. [115] synthesized NiS nanoframes utilizing Ni–Co Prussian blue analogue nanocubes as a matrix. These NiS nanostructures showed a superior capacitance of 2384 $F \cdot g^{-1}$ at 1 $A \cdot g^{-1}$. This extraordinary pseudocapacitive behavior is possibly credited to the high surface area/volume ratio with the distinctive 3D frame-like hollow porous structure, which provides a huge electrode–electrolyte interaction. You et al. [116] prepared hierarchical porous NiS superstructures (h-NiS$_x$) by the electrodeposition method and obtained an excellent areal specific capacitance of 6104 $mF \cdot cm^{-2}$ at a scan rate 10 $mV \cdot s^{-1}$, besides the amazing cycle stability. The h-NiS$_x$ accompanied by three-dimensional (3D) hierarchical structures composed of diffused, interconnected macropores and mesopores enables bountiful electrolyte-accessible channels, and the reduced ion diffusion length is responsible for high capacitive performance. The hierarchical NiS microflowers designed to utilize Ni(OH)$_2$ as a precursor by sulfuration method [117] delivered a remarkable specific capacitance of 1123 $F \cdot g^{-1}$ at a current density of 1 $A \cdot g^{-1}$ along with 97.8% retention in specific capacitance at 10 $A \cdot g^{-1}$ over 1000 charge–discharge cycles. High porosity and huge specific surface area created by unique NiS microflower structure, which promote the electron transfer and electrolyte insertion/de-insertion, are accountable for the excellent capacitive performance. Surendran et al. [118] prepared the arrays of flower-like β-NiS nanostructures on flexible carbon cloth (β-NiS@CC), which showed an extraordinary areal capacity of 1.654 $C \cdot cm^{-2}$ (827 $C \cdot g^{-1}$) at 1 $mA \cdot cm^{-2}$. Du et al. [119] synthesized NiS double-shelled hollow structures using α-Fe$_2$O$_3$ as template. The nanosheet-assembled shells produced open huge mesopores, which could enable transportation of the electrolyte and ions. Among them, capsule-shaped NiS exhibited an outstanding capacitance of 1159 $F \cdot g^{-1}$ at a rate of 2 $A \cdot g^{-1}$ in three-electrode system. The corresponding NiS//rGO@Fe$_3$O$_4$ hybrid asymmetric supercapacitor (ASC) showed a specific capacitance of 122.8 $F \cdot g^{-1}$ at a current density of 0.83 $A \cdot g^{-1}$. Yang et al. [120] introduced the synthesis of hierarchical flower-like β-NiS spheres through a solvothermal template-free approach, which delivered specific capacitances of 972.3

and 729.7 $F \cdot g^{-1}$ at current densities of 2 and 15 $A \cdot g^{-1}$, respectively, and showed a capacitance of 778.8 $F \cdot g^{-1}$ after 3000 cycles at the current density of 4 $A \cdot g^{-1}$, indicating excellent rate capability. This remarkable capacitive performance is due to the hierarchical flower-like framework assembled by nanoplates, which offers plenty of reactive sites for charge–discharge route. Uniform NiS hierarchical hollow cubes are also designed from Ni-formate framework through a hydrothermal process based on Kirkendall effect and Ostwald ripening [121]. These electrodes reveal a capacitance of 874.5 $F \cdot g^{-1}$ at 1 $A \cdot g^{-1}$ along with 90.2% retaining capacitance even 3000 charge–discharge cycles. Additionally, NiS//CNFs in asymmetric configuration showed an energy density of 34.9 $W \cdot kg^{-1}$ at a power density of 387.5 $W \cdot kg^{-1}$.

3.2 NiS composites

Aforementioned research investigations on nickel sulfide materials illustrate that those special nanostructures are skilled to raise the electrochemical performance for SCs. Nickel sulfides generally exhibit higher specific capacitance than carbon-based electrodes, but they have some drawbacks, such as poor electrical conductivity and particle agglomeration, which crucially limit their demands in SCs [122]. To extensively combine the carbonaceous materials with potential benefits and pseudocapacitive materials, the construction of functional nanomaterials on carbonaceous materials including graphene, carbon nanotubes and carbon fiber is an impressive strategy to enhance the electrochemical behavior described with cycling life and rate capability [123, 124]. Up to date, various NiS hybrids such as NiS/hollow carbon spheres (HCSs) have been proved to be potential electrode materials [125], where the internal space provides ion channels for fast electrochemical reactions, the carbon shell assists in electron transport and the huge surface area recommends the discharge of active materials. Accordingly, a narrow and porous layer of active material expanded on the hollow carbon spheres surface could raise energy storage and rate capacity. Structure and synthesis of NiS porous nanosheets coated on N-doped hollow carbon spheres (NHCSs) by well-organized template-assisted route are investigated for SCs [125]. Core–shell structures of NHCSs@SiO$_2$ serving as a template for nickel silicates further yield NiS/NHCS hollow structures followed by the formation of NHCS-reinforced NiS nanosheets (NiS/NHCS). Charge–discharge profiles of NiS/NHCS and NiS hollow spheres (NiS/HS) exhibited reversible Faradaic redox processes. The NiS/NHCS electrode shows a favorable capacitance of 1150 $F \cdot g^{-1}$ at a current density of 1 $A \cdot g^{-1}$ and a capacitance retention of 52.2% at 20 $A \cdot g^{-1}$, as well as 76% at 5 $A \cdot g^{-1}$ over 4000 charge–discharge cycles. Furthermore, the hybrid

supercapacitor of NiS/NHCS//AC performed a high capacitance of 120 $F \cdot g^{-1}$ at 0.2 $A \cdot g^{-1}$ and maintained a capacitance of 46 $F \cdot g^{-1}$ at 5 $A \cdot g^{-1}$.

The incorporation of hierarchically porous electrodes and conductive substrates/frameworks may exhibit synergistic effects for enhanced performances [126, 127]. Recently, metal–organic frameworks (MOFs) are widely used as an emerging template for the fabrication of active materials because MOFs could be easily transformed into battery-type materials or carbon-based materials with large surface areas [126, 127]. The combination of MOFs-derived composites and graphene sheets is expected to provide adequate electrical affinity between the discrete electroactive particles and shorten the ionic transport path. Qu et al. [109] designed and fabricated a hierarchically porous hybrid electrode of α-NiS nanorods decorated on reduced graphene oxide (R-NiS/rGO) (Fig. 2a), deriving from water-refluxed Ni-MOF-74/rGO template. The obtained R-NiS/rGO shows a low charge-transfer resistance of 1.41 Ω, presenting good conductivity, which is attributed to the intimate contact of conductive rGO with NiS (Fig. 2b). The R-NiS/rGO hybrid composite electrode delivers a capacity of 744 $C \cdot g^{-1}$ at 1 $A \cdot g^{-1}$ and an extraordinary rate performance (600 $C \cdot g^{-1}$ at 50 $A \cdot g^{-1}$), and it preserves more than 89% of the initial capacity over 20,000 cycles (Fig. 2c). These results indicate that the MOF-extracted α-NiS nanorods with abundantly available electrolyte-accessible surfaces are beneficial to fast redox reactions in an alkaline electrolyte. Furthermore, when coupled with a negative electrode of N-doped graphene aerogel (C/NG-A), the hybrid supercapacitor exhibits a high energy density of 93 $W \cdot kg^{-1}$ at a power density of 962 $W \cdot kg^{-1}$ (Fig. 2d).

AbdelHamid et al. [123] synthesized graphene-wrapped NiS nanoprisms that showed excellent capacitance of 1337 and 778 $F \cdot g^{-1}$ at current densities of 3 and 20 $A \cdot g^{-1}$, respectively, indicating remarkable rate capability. This excellent capacitive performance results from the direct anchoring of NiS nanoprisms on the surface of graphene sheets, which ultimately facilitates electronic transport; furthermore, the larger surface area and porosity of the nanocomposite expedite the electrolyte transport and ionic
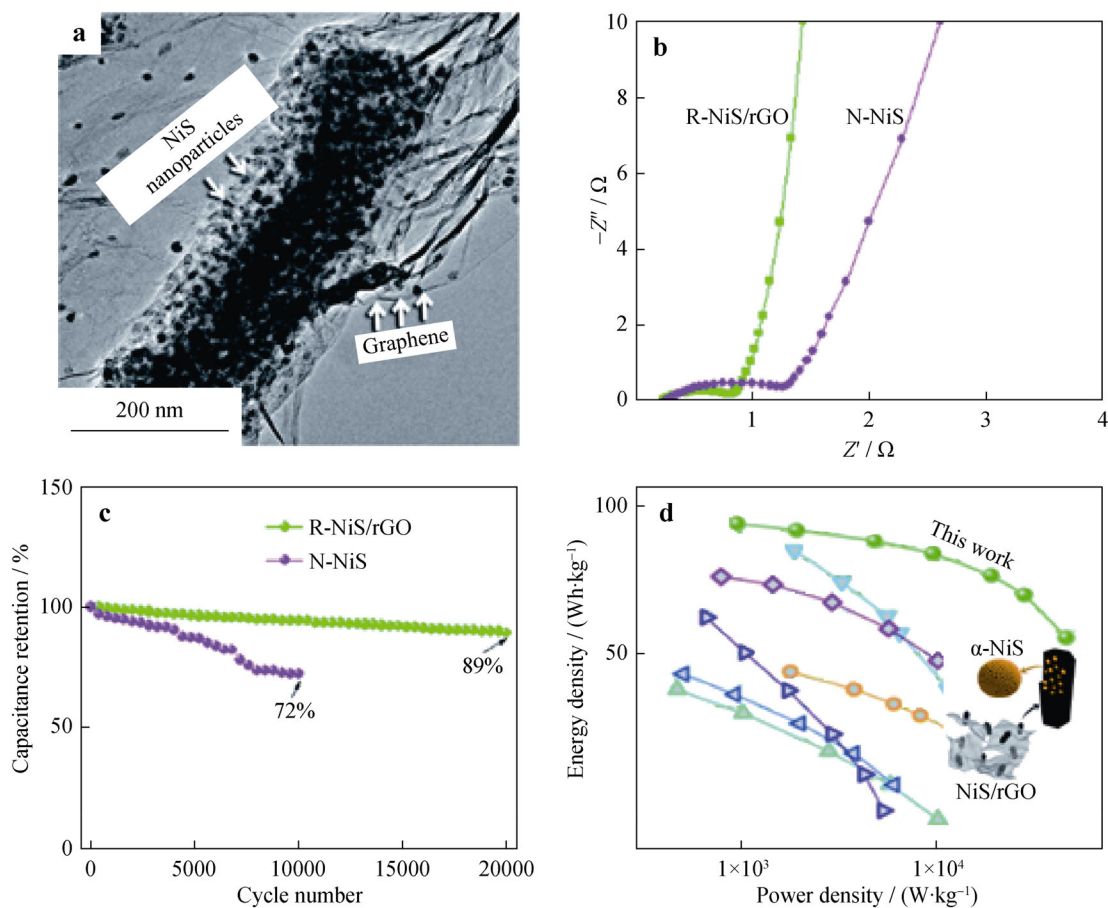

Fig. 2 **a** TEM image of R-NiS/rGO; **b** Nyquist plots and **c** cycling performances of R-NiS/rGO and N-NiS; **d** comparison of Ragone plots of R-NiS/rGO//C/NG-A and other recently reported high-performance hybrid/asymmetric SCs. (reproduced from Ref. [109], Copyright 2018 The Royal Society of Chemistry)

diffusion, which enhances the rate capability of the electrode. Sun et al. [106] demonstrated a simple in situ sulfuration and phase-controlled process for α-NiS nanoparticles inserted in carbon nanorods (α-NiS/CRs). This hybrid composite electrode material exhibits high specific capacitance (1092 and 740 $F \cdot g^{-1}$ at 1 and 10 $A \cdot g^{-1}$, respectively) with superior cycling life (with no capacitance decrease after 2000 cycles). Singh et al. [124] hydrothermally synthesized MWCNTs/NiS (MWNS) composite and graphene nanoplatelets, which were used as electrode materials for the positive and negative electrodes. The MWCNT/NiS//graphene nanoplatelets-based ASC exhibited a specific capacitance of 181 $F \cdot g^{-1}$ at a current density of 1 $A \cdot g^{-1}$. The ASC also presented 92% retention of initial capacitance after 1000 cycles at 2 $A \cdot g^{-1}$. The improved capacitive performance results from the enhanced conductivity and large surface area of MWNS, which enable deeper penetration of electrolyte ions into electrode materials and electrochemical activity enhancement of the graphene sheet film. Li et al. [128] chose the commercial flexible makeup cottons (MCs) as skeleton to fabricate 3D interconnected graphene-wrapped macro-networks with NiS (MCs@GNS@NiS), which were synthesized by "dip and dry" and electrodeposition technique. This MCs@GNS@NiS electrode demonstrates a high specific capacitance of 775 $F \cdot g^{-1}$ at a current density of 0.5 $A \cdot g^{-1}$ and 88.1% retention in capacitance after 1000 cycles at 2 $A \cdot g^{-1}$; it also delivers a high energy density of 11.2 $W \cdot kg^{-1}$ at a high power density of 1008 $W \cdot kg^{-1}$. This high capacitive achievement is assigned to its special homogeneous 3D networks that are favorable for the access of electrolytes to active electrode materials. Zhang et al. [129] reported a one-step solvothermal reaction for NiS/N-doped carbon fiber aerogel (N-CFA) nanocomposite. The optimized NiS/N-CFA nanocomposite delivers a large specific capacitance of 1613 $F \cdot g^{-1}$ at 1 $A \cdot g^{-1}$ and shows 87.0% retention in capacitance after 5000 cyclic voltammetry cycles at a scan rate of 20 $mV \cdot s^{-1}$ as well as 66.7% retention in capacitance at 20 $A \cdot g^{-1}$.

4 NiS_2

4.1 Pristine NiS_2

Recently, nonnoble metal chalcogenides including NiS_2 have attracted great interest owing to their large energy storage capacity and catalytic activity [130]. However, the inferior cycling performance of NiS_2-based electrode materials hampers their application in SCs [131]. To solve these problems especially durability and sluggish redox kinetics, metal doping into the lattice of NiS_2 is proved to be an effective strategy. Well-organized charge transfer between the doped metal element and host as well as the modification of the electronic environment can decrease

the kinetic resistance during the charge–discharge process and favor an enhancement in electrochemical performance [132]. Xie et al. [132] fabricated a Co-doped nickel disulfide ($Ni_xCo_{1-x}S_2$) nanostructure via a facile solvothermal process. The fluffy structure of $Ni_{0.75}Co_{0.25}S_2$ facilitates the contact between the electrolyte and electrode material during the charging/discharging process. Transmission electron microscopy (TEM) image of $Ni_{0.75}Co_{0.25}S_2$ reveals that most hollow spheres were broken into uniform nanoparticles with numerous active edge sites (Fig. 3a). The $Ni_{0.75}Co_{0.25}S_2$ sample demonstrates an excellent specific capacitance of 2141.9 $F \cdot g^{-1}$ at a current density of 2 $A \cdot g^{-1}$ (Fig. 3b), as well as a highest energy density of 54.9 $W \cdot kg^{-1}$ and enhanced cycle life (85.1% capacitance retained over 4000 cycles).

Low-dimensional nanomaterials have high surface area and short electron transport pathway for enhanced performance [133]. Ruan et al. [134] developed a simple facile solution process to fabricate square rod-like NiS_2 precursor with open ends (Fig. 3c). In contradiction to the traditional hydrothermal route for specific materials structure with numerous conditional inhibitions, this process can be smoothly conducted in favorable innovative circumstances and extended to other metal sulfide precursors. Self-assembly synthesis of the square rod-like NiS_2 precursor depends on the reaction time, which is represented by TEM image (Fig. 3d). The porous NiS_2 square rods achieved via an annealing process showed high specific capacitances of 1020.2, 534.9 $F \cdot g^{-1}$ at 1 and 10 $A \cdot g^{-1}$, respectively, as well as long cycle stability (93.4% retention of the initial specific capacitance over 1000 cycles). Moreover, ASC device using NiS_2 as the cathode and rGO as the anode reveals a high energy density of 32.8 $W \cdot kg^{-1}$ at a power density of 954 $W \cdot kg^{-1}$ (Fig. 3e). Lu et al. [130] reported that NiS, NiO and $NiSe_2$ with the unique hollow structure could be obtained based on NiS_2 hollow spheres through the L-cysteine-assisted hydrothermal method. Specific capacitances of the NiS_2, NiS, NiO and $NiSe_2$ electrodes were 1643, 1076, 581 and 341 $F \cdot g^{-1}$, respectively, at a rate of 1 $A \cdot g^{-1}$. The consequences indicated that both the NiS_2 and NiS electrodes displayed the highest specific capacitance, while the NiO and $NiSe_2$ electrodes exhibited long cycling stability. To achieve larger specific surface area with more exposed active sites for fast ion/electrolyte transfer, Ni et al. [135] synthesized foam-like hierarchical structures of ultrathin NiS_2 nanosheets epitaxially grown on their homogeneous nanowire backbones by one-pot reaction (i.e., controlled nucleation and growth process) and subsequent sulfidation (Fig. 4a–d). The as-synthesized hierarchical NiS_2 demonstrated a high pseudocapacitance of 1788 $F \cdot g^{-1}$ at a current density of 0.3 $A \cdot g^{-1}$, as well as superior rate capacitance of 1223 and 750 $F \cdot g^{-1}$ at 10 and 30 $A \cdot g^{-1}$, respectively (Fig. 4e) [135].
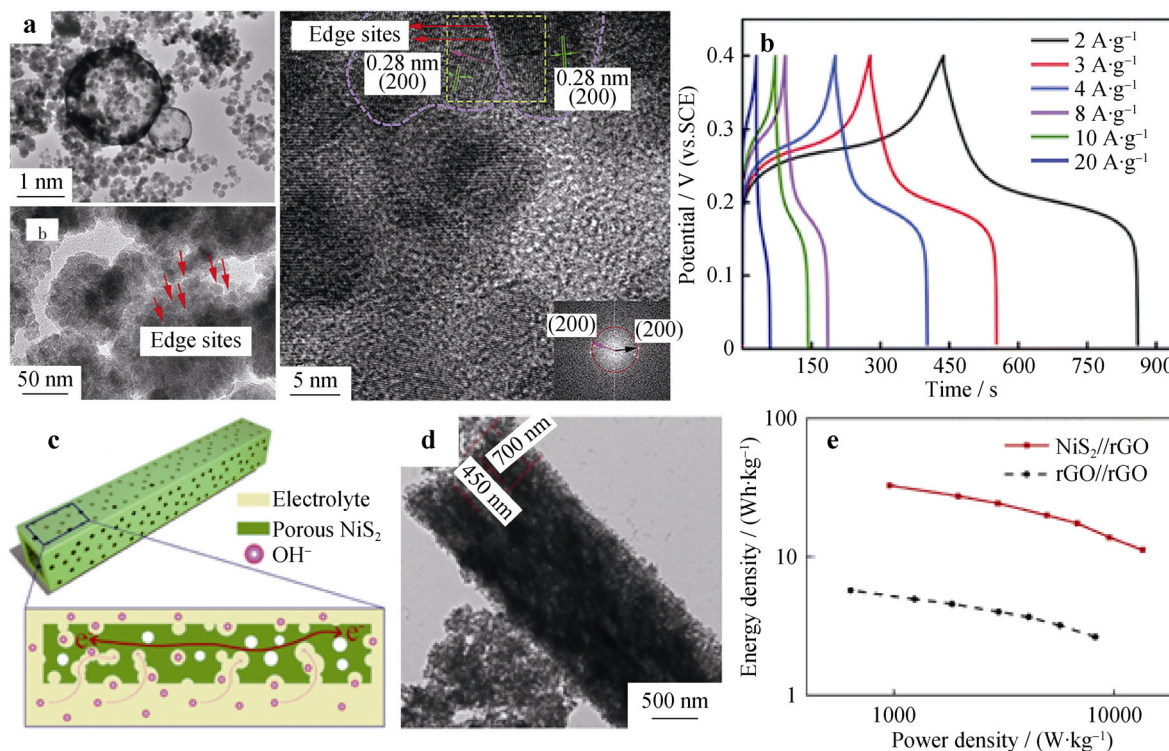
Fig. 3 a TEM and HRTEM images of $Ni_{0.75}Co_{0.25}S_2$ sample (inset being fast Fourier transform (FFT) image) and **b** galvanostatic charge/discharge (GCD) curves of $Ni_{0.75}Co_{0.25}S_2$. (reproduced from Ref. [132], Copyright 2018 The Royal Society of Chemistry and the Partner Organisations); **c** schematic diagram representing electronic transport pathway and electrolyte ions dissemination in porous NiS_2 electrode; **d** TEM image of NiS_2 and **e** Ragone plots of NiS_2//rGO ASC and the rGO//rGO symmetric SC. (reproduced from Ref. [134]. Copyright 2015 Elsevier)

4.2 NiS$_2$ composites

Some other transition-metal-based composite electrode materials for supercapacitors have been reported for improving the electrical conductivity and cycle stability of Ni-based materials due to the strong coupling effects between different components [55, 104, 136, 137]. Furthermore, the phase boundaries in these composites could create highly active sites for redox reaction and thus lead to improved electrochemical performance [138]. Gou et al. [138] prepared hollow spherical Ni_2P/NiS_2 composite (Fig. 5a) by a simple hydrothermal route, which shows capacitances of 212.7, 181.7, 159.4, 148.7 and 120.9 mAh·g^{-1} at various current densities of 2, 4, 8, 10, and 20 A·g^{-1}, respectively (Fig. 5b). Ni_2P/NiS_2 composite demonstrates higher pseudocapacitance than bare NiS_2 and Ni_2P due to their synergistic contribution (Fig. 5c), exhibiting a fair cycling life (maintaining a gravimetric capacity of 118.9 mAh·g^{-1} after 5000 cycles at a current density of 2 A·g^{-1}), as well as high rate capacitance with 83.6% retention of the starting capacity up to 10 A·g^{-1} (Fig. 5d). Li et al. [139] synthesized a 3D graphene-modified NiS_2 nanocomposite (graphene/NiS_2) with high surface area, improved electrical conductivity, good

mechanical strength and stable crystal structure by a template-free solvothermal method. The graphene/NiS_2 composite displays a specific capacitance of 478.1 F·g^{-1} at 0.5 A·g^{-1}. After 2000 cycles, the composite decays only 10.7% of its initial value. Ji et al. [140] established a heterostructure material of core–shell $MnO_2@NiS_2/Ni(OH)_2$ by a two-step hydrothermal route at various temperatures. The as-prepared heterostructure composite consists of 1D MnO_2 nanosticks and 2D $NiS_2/Ni(OH)_2$ sheets as pseudocapacitive materials, exhibiting a large specific capacitance of 1010 F·g^{-1} at 1 A·g^{-1} and an enhanced cycling capacitance of 785 F·g^{-1}, i.e., 78% capacity retention after 3000 cycles.

5 Ni$_3$S$_2$

5.1 Pristine Ni$_3$S$_2$

Ni_3S_2 is one of the most crucial phases of nickel sulfides, and it provides many virtues such as excellent theoretical capacitance (2412 F·g^{-1}), outstanding redox features and high conductivity, which are promising for practical energy storage systems [141]. In addition, Ni_3S_2 is of low cost,
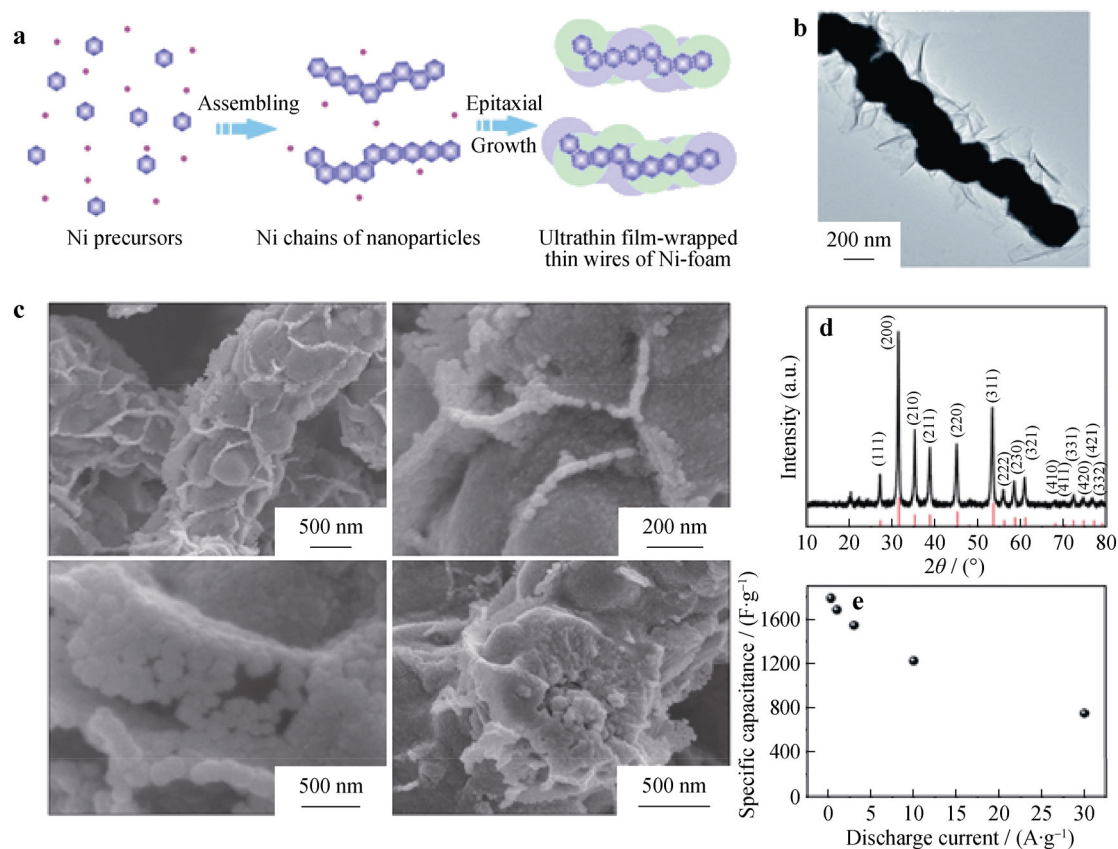
Fig. 4 **a** Schematic diagram of one-pot synthesis for foam-like hierarchical structure of Ni nanosheets-wrapped nanowires (i.e., Ni ultrathin lamella wrapped chainlike backbone), and **b** corresponding TEM image; **c** SEM images and **d** X-ray diffraction (XRD) pattern of as-synthesized hierarchical NiS_2 nanofoam, and **e** related specific capacitance at various current densities. (reproduced from Ref. [135], Copyright 2014 The Royal Society of Chemistry)

natural abundance and environmental benignity. Ni_3S_2 shows intrinsic metallic behavior resulting from its extended network of Ni–Ni bond structures [142]. Furthermore, these nickel sulfide nanostructures can be easily obtained through general chemical reactions with controllable morphologies including nanowires, nanorods, nanoneedles and nanosheets [143, 144]. Therefore, to generate an enhanced supercapacitive performance, a rational design of Ni_3S_2 nanostructures with abundant surface electroactive sites is required. For example, as a novel category of flexible energy storage devices, fiber-type supercapacitors have gained intense awareness due to their advantages of fairly large capacitance density, flexibility and facile incorporation with different electronic devices, viz., they could be precisely used as wearable and portable device units and can be simply designed into different structures for new design and readily combined with a variety of electronic devices [145]. For example, Wen et al. [145] fabricated a new coaxial-type flexible fiber asymmetrical supercapacitor (ASC) using Ni_3S_2 nanorod arrays and pen ink as positive and negative electrode materials, respectively. The Ni_3S_2 nanorod array used as electrode material

in fiber SCs was directly spread on Ni wire via hydrothermal route, and a simple dip-coating method was used to develop the pen ink/Ni electrode. At the voltage range of 0–0.5 V, the Ni_3S_2 nanorod arrays/nickel wire shows similar redox peaks in CV curves at scan rates from 10 to 100 $mV·s^{-1}$, revealing high reversible reaction on the surface of Ni_3S_2 electrode. The constructed ASC device shows a specific capacitance of 34.9 $F·g^{-1}$ (87.3 $F·cm^{-1}$) at a scan rate of 10 $mV·s^{-1}$. The ASC device can work robustly within a voltage window of 0–1.4 V and deliver a high energy density of 8.2 $W·kg^{-1}$ (0.81 $mWh·cm^{-3}$) and a power density of 214.6 $W·kg^{-1}$ (21.1 $mW·cm^{-3}$). To further improve the application of metal sulfides, different nanostructures have been instantly grown on 3D porous current collectors to construct large surface areas, short electron- and ion-transport pathways and outstanding rate capability and cycle performance. Xiong et al. introduced a unique electrode framework made up of Ni_3S_2 nanosheet-onto-Ni_3S_2 nanorods spread on nickel foam through a simple one-step hydrothermal method (Fig. 6a) [146]. The Ni_3S_2 nanosheet@nanorods electrode exhibited an initial capacity of 489 $F·g^{-1}$ and maintained 89.3% retention after
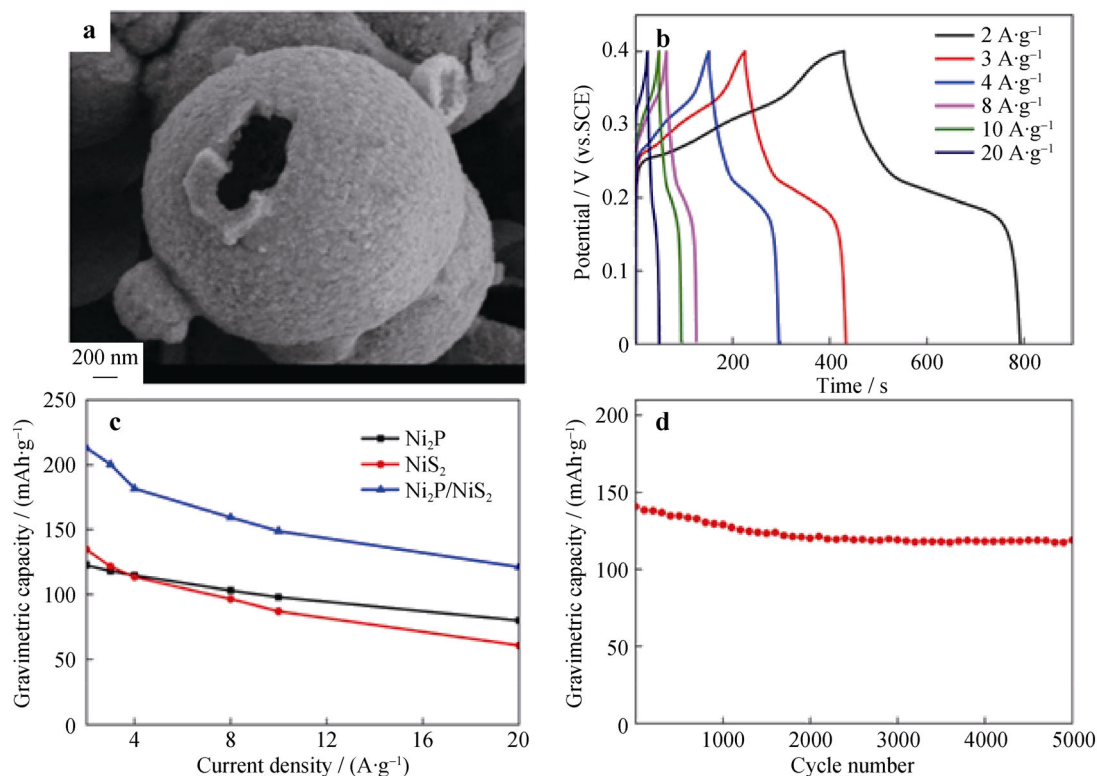
Fig. 5 **a** SEM image and **b** GCD curves at various current densities of Ni_2P/NiS_2 composite; **c** gravimetric capacities of Ni_2P, NiS_2 and Ni_2P/NiS_2; **d** cycle performance of Ni_2P/NiS_2 composite at current density of 10 $A \cdot g^{-1}$ over 5000 cycles. (reproduced from Ref. [138], Copyright 2017 The Electrochemical Society)

5000 cycles (Fig. 6b) at a cycling rate of 120 $mA \cdot cm^{-2}$, as well as a specific capacitance decrease by $< 42\%$ with increased current density from 20 to 240 $mA \cdot cm^{-2}$, indicating good rate capability. Ni_3S_2 nanosheet@Ni_3S_2 nanorods electrode for ASC, with a high loading density of 5.8 $mg \cdot cm^{-2}$, displays an optimized volumetric energy density of 1.96 $mWh \cdot cm^{-3}$ at 1.2 $A \cdot g^{-1}$ and a power density of 0.6 $W \cdot cm^{-3}$ at 28.3 $A \cdot g^{-1}$ (bridging the performance gap between thin-film Li batteries and commercial AC//AC supercapacitors) (Fig. 6c), as well as an excellent cycle stability over 5000 cycles (Fig. 6d). This remarkable capacitive achievement is assigned to the adequate mechanical friction and electrical attachment with the substrate, superior contact area with electrolyte and prevented structural pulverization through the cyclic process. To clearly indicate various parameters on performance, a series of typical Ni_3S_2 nanostructures with different morphologies obtained by different synthesis methods is shown in Table 1 [147–156].

5.2 Ni_3S_2/TMC composites

Numerous techniques have been practiced to enhance the behavior of energy storage devices through the evolution of new electrode materials. The fabrication of transition-metal

compound (TMC) composite electrodes plays a vital role in improving the performance of energy storage devices [157, 158]. Bimetallic sulfides possess richer redox reactions than their single-component counterparts, resulting in superior specific capacitance [157], and bimetallic sulfide species can also be readily restored from their metal oxide/ hydroxide precursors via anion exchange reactions or Kirkendall effects and finally lead to multiform and controllable morphologies (e.g., nanowires, nanotubes and nanosheets). Thus, developing rational nanostructures for upgraded pseudocapacitive electrodes can not only increase the electrical conductivity and the utilization of atoms, but also shorten the electron/ion diffusion path. In this manner, ultrathin and porous Ni_3S_2/$CoNi_2S_4$ 3D network grown on Ni foam (Ni_3S_2/$CoNi_2S_4$/NF) was synthesized by a sulfidation process using 3D-networked Ni–Co precursor (Ni–Co precursor/NF) [157]. The SEM images show that surfaces of sulfuretted nanosheets become rough due to the formation of nanoparticles on the surface (Fig. 7a, b). Ni_3S_2/ $CoNi_2S_4$/NF 3D networked electrode can deliver a specific capacitance of 2435 $F \cdot g^{-1}$ at 2 $A \cdot g^{-1}$ (Fig. 7c) and a notable rate capability of 80% retention at 20 $A \cdot g^{-1}$. Additionally, the as-prepared hybrid capacitor demonstrates a superior capacitance (175 $F \cdot g^{-1}$ at 1 $A \cdot g^{-1}$) and an energy density of 40.0 $W \cdot kg^{-1}$ at a power density of 17.3 $kW \cdot kg^{-1}$.
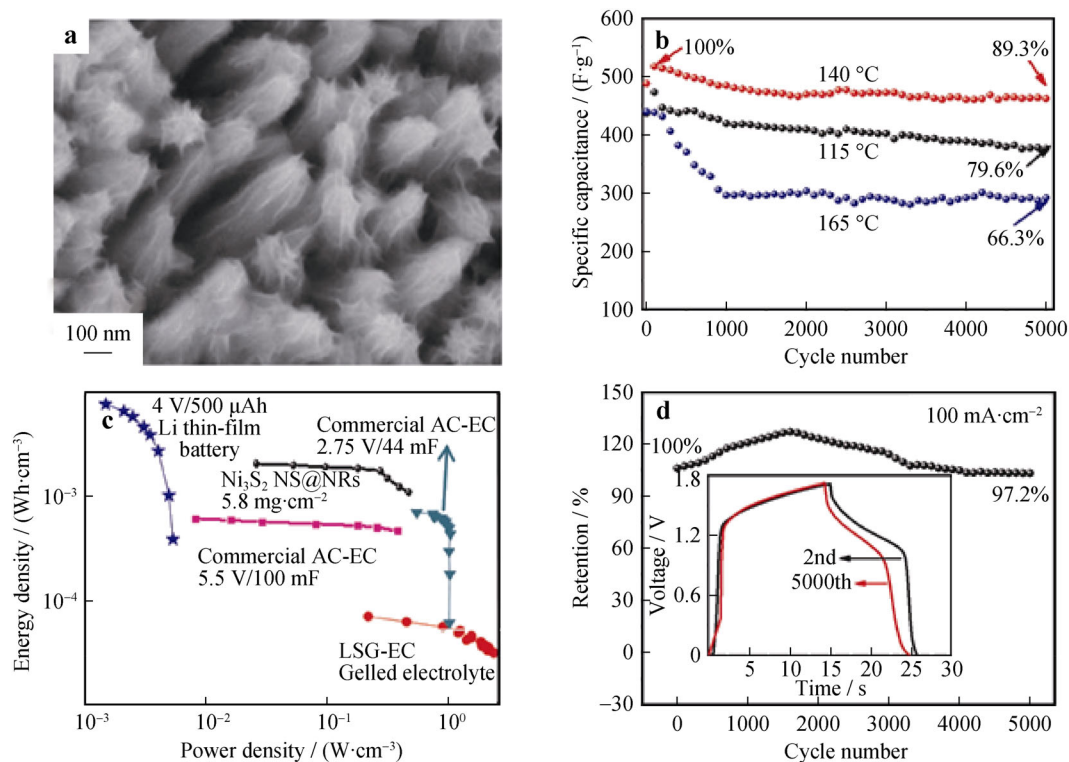
Fig. 6 **a** SEM image and **b** specific capacitance at various current densities of Ni_3S_2 nanosheet@nanorods (NS@NRs); **c** comparison of volumetric power density of Ni_3S_2 NS@NRs ASC electrode with other reported ECs/batteries data (i.e., laser-scribed graphene (LSG) EC, Li thin-film battery and commercial AC//AC EC with typical parameters); **d** cycle stability of Ni_3S_2 nanosheet@nanorods//AC. (reproduced from Ref. [146]. Copyright 2016 Springer Nature)

An emerging approach to increase the electrochemical performance of nickel sulfides is to combine with $NiCo_2O_4$ arrays [158]. For instance, 3D hierarchical $NiCo_2O_4@$-Ni_3S_2 core/shell arrays on Ni foam were prepared via a stepwise process (Fig. 7d) [158]. The 3D heterogeneous $NiCo_2O_4$ nanoarchitecture generates an interconnected web-like platform and acts as the core inside Ni_3S_2 shell. The $NiCo_2O_4@Ni_3S_2$ nanowire array electrodes demonstrate significant electrochemical performance, e.g., optimal specific areal capacitance of 3.0 $F·cm^{-2}$ at a current density of 5 $mA·cm^{-2}$ and good cycling stability of 93.3% retention in capacitance after 10,000 cycles (Fig. 7e). The $NiCo_2O_4@Ni_3S_2$//AC solid-state ASC device displays a high energy density of 1.89 $mW·cm^{-3}$ at 5.81 $W·cm^{-3}$ and a high power density of 56.33 $W·cm^{-3}$ at 0.94 $mW·cm^{-3}$ (Fig. 7f). The synthesis of TMC composites usually integrates the benefits of their constituent materials, resulting in a synergistic effect. The phase interface existing in a composite often leads to lattice mismatch and therefore creates more active sites for energy storage, allowing the electrodes to exceed their theoretical capacity. The synergistic effect generated from the composite interface boundaries and pseudocapacitance contributions could display excellent diffusion-controlled capacity performance even at a higher rate [157–159]. In consideration of

these favorable conditions, Long et al. [159] synthesized $Ni_3N@Ni_3S_2$ nanosheets composite by calcinating Ni-based precursor in ammonia followed by sulfuration. Ni_3S_2 is preferred over NiO due to the better conductivity of sulfides than oxides. $Ni_3N@Ni_3S_2$ nanosheets showed an excellent capacitance of 849 $F·g^{-1}$ at a current density of 6.25 $A·g^{-1}$ and 89% retention in capacitance after 15,000 long-term charge–discharge cycles.

5.3 Ni_3S_2/carbon composites

Fabrication of hybrid capacitors by direct growth of pseudocapacitive materials on a conducting matrix, e.g., graphene, porous Ni foam, is a promising alternative to increase the electrical conductivity and cyclic stability of pseudocapacitor electrodes [160, 161], which will not only eliminate the side effects and complications arising from the use of binders but also produce a promising free-standing electrode of large contact area with the electrolyte, potentially contributing to the improved electrochemical performance [162]. Three-dimensional nanostructures are considered as one of the most prominent electrode materials for SCs, which possess a short path for ion diffusion and huge surface area enabling adequate association between the electrolyte ions and the active

Table 1 Electrochemical performances of typical Ni_3S_2 and their hybrid nanostructures

Samples	Methods	Electrolyte	Specific capacitance	Cycle life[a]	Refs.
Nest-like hierarchical Ni_3S_2	Hydrothermal	1 mol·L^{-1} NaOH	1293 F·g^{-1} at 5 mA·cm^{-2}	69%/1000/ 25 mA·cm^{-2}	[147]
Ni_3S_2 flakes	Potentiodynamic electrodeposition	1 mol·L^{-1} KOH	717 F·g^{-1} at 2 A·g^{-1}	91%/1000/ 4 A·g^{-1}	[148]
3D Ni_3S_2 nanosheet arrays	Hydrothermal	6 mol·L^{-1} KOH	1370.4 F·g^{-1} at 2 A·g^{-1}	91.4%/1000/ 6 A·g^{-1}	[149]
Ni_3S_2 flakes	Potentiodynamic & pulse-reversal electrodeposition	1 mol·L^{-1} KOH	179.5 mAh·g^{-1} at 2 A·g^{-1}	97%/1000/ 2 A·g^{-1}	[150]
Grass-like Ni_3S_2 nanorod/nanowire arrays	Hydrothermal	3 mol·L^{-1} KOH	4.52 F·cm^{-2} at 1.25 mA·cm^{-2}	108%/2000/ 1.25 mA·cm^{-2}	[151]
Nanoporous net-like Ni_3S_2 thin films	Pulse-reversal electrodeposition	1 mol·L^{-1} KOH	7.25 F·cm^{-2} at 5 mA·cm^{-2}	77%/5000/ 0.05 mA·cm^{-2}	[152]
$Mo_2S_3@Ni_3S_2$ nanowires	Hydrothermal	6 mol·L^{-1} KOH	998.9 F·g^{-1} at 1 A·g^{-1}	90.6%/650/ 2 A·g^{-1}	[153]
V_2O_5/Ni_3S_2 nanoflakes	Hydrothermal	2 mol·L^{-1} NaOH	4.2 F·cm^{-2} at 5 mA·cm^{-2}	85%/2500/ 10 mA·cm^{-2}	[154]
Clustered network-like Ni_3S_2–Co_9S_8	Solvothermal	6 mol·L^{-1} KOH	5.37 F·cm^{-2} at 5 mA·cm^{-2}	92%/1000/ 5 mA·cm^{-2}	[155]
Hierarchical $Co_3O_4@Ni_3S_2$ core/shell nanowire arrays	Hydrothermal	3 mol·L^{-1} KOH	1710 F·g^{-1} at 1 A·g^{-1}	85%/1000/ 4 A·g^{-1}	[156]

[a]Retention/cycles/current density

materials [161]. Three-dimensional graphene network (3DGN) grown on nickel foam is an ideal template for the construction of graphene-based composite electrodes and pseudocapacitor electrode materials [161]. Inspired from the advantages of 3DGN integration with pseudocapacitive materials including nickel sulfides and layer-structured nickel hydroxide, Zhou et al. [161] prepared a Ni_3S_2 nanorod@$Ni(OH)_2$ nanosheet core–shell nanostructure spread on a 3DGN/nickel foam through a facile hydrothermal process, and morphology evolution and growth mechanism were discussed. This $Ni_3S_2@Ni(OH)_2$/ 3DGN electrode delivers a high capacitance of 1037.5 F·g^{-1} at 5.1 A·g^{-1} and 3.85 F·cm^{-2} at 19.1 mA·cm^{-2} along with 99.1% retention in capacitance after 2000 cycles. In addition, core–shell nanostructures with a controllable material constitution and utility could also help to increase both conductivity and charge storage capability in electrodes of energy storage devices. For example, a conductive core could enhance the charge conduction within the material, while a shell made of porous materials could provide preferable contact with ions at the electrode–electrolyte interface and buffer the volume changes during the charge–discharge process. Hierarchical carbon@Ni_3S_2@MoS_2 double core–shell nanorods have been designed and prepared with the assistance of carbon/ Ni nanorods serving as template and precursor [160]. This unique architecture improves the connection area with electrolyte and significantly enhances the capacitance along with the protection from the conductive core material

in redox reactions. As a result, the C@Ni_3S_2@MoS_2 double core–shell nanorods display a specific capacitance of 1544 F·g^{-1} at a current density of 2 A·g^{-1}, and outstanding cycle stability (92.8% retained capacitance after 2000 cycles at 20 A·g^{-1}).

6 Ni_3S_4

6.1 Pristine Ni_3S_4

Among all kinds of Ni_xS_y, Ni_3S_4 shows outstanding redox reversibility, safety and marvelous specific capacitance [82, 163]. Pristine Ni_3S_4 nanoparticles can deliver a specific capacitance of 1226.5 F·g^{-1} and 71.8% capacitance retention after 1000 cycles [164]. Wang et al. [165] synthesized rigid 3D Ni_3S_4 nanosheet frames via the hydrothermal method, demonstrating a high specific capacitance of 1213 F·g^{-1} and a capacitance retention of about 60% over 2000 cycles. In addition, to improve their supercapacitive properties, design and fabrication of hybrid nanomaterials are considered to be successful approaches. By hybridizing other active materials with nickel sulfides, cycling stability can be increased. However, in the practical approach, those electrodes are restricted in flexibility. Huang et al. [166] synthesized Ni_3S_4 on the surface of carbon cloth (CC) through a facile one-step hydrothermal process. CC will provide not only superior device flexibility but also a 3D scaffold for the diffusion of ions. The
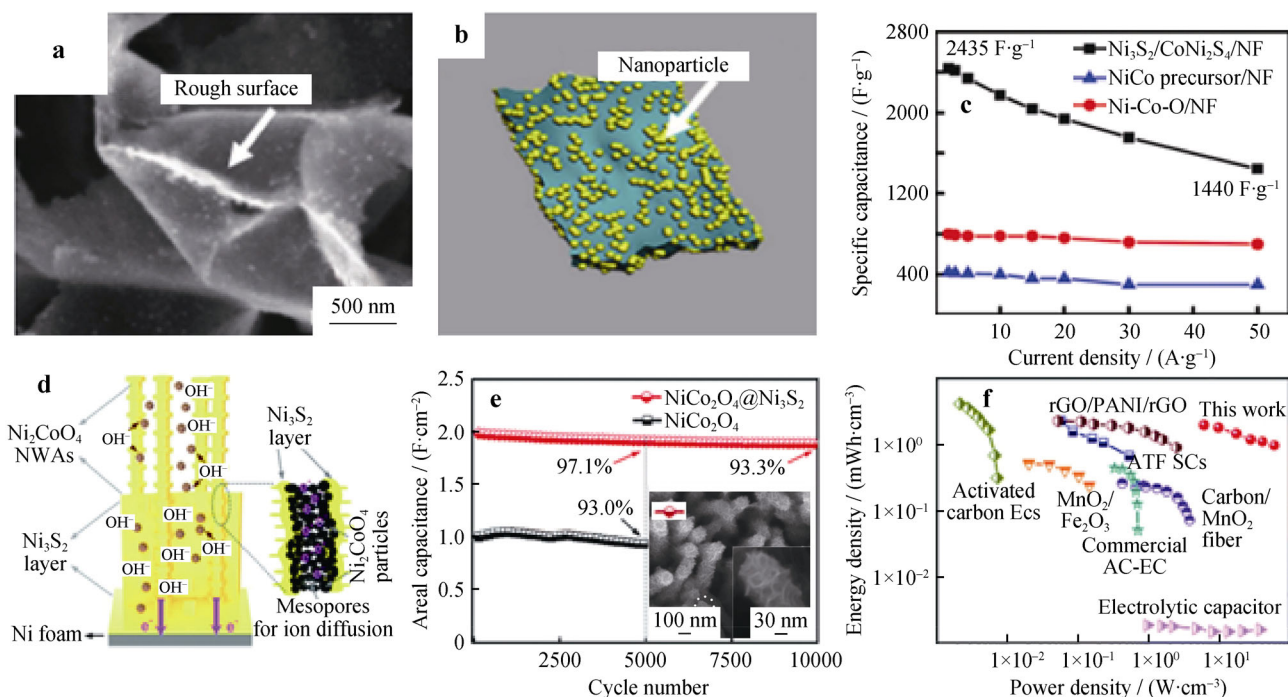
Fig. 7 **a** SEM image and **b** structural diagram of $Ni_3S_2/CoNi_2S_4/NF$; **c** specific capacitances of $Ni_3S_2/CoNi_2S_4/NF$, Ni–Co oxide/NF and Ni–Co precursor/NF at different current densities (reproduced from Ref. [157]. Copyright 2017 WILEY–VCH); **d** schematic diagram of $NiCo_2O_4@Ni_3S_2$ hybrid nanostructure; **e** cycling performance of $NiCo_2O_4$ and $NiCo_2O_4@Ni_3S_2$ electrodes; **f** Ragone plot of $Ni_3S_2/CoNi_2S_4/NF$ based ASC device compared with other reported ASC devices. (reproduced from Ref. [158], Copyright 2016 The Royal Society of Chemistry)

as-prepared flexible Ni_3S_4/CC electrode demonstrates an excellent specific performance of 1340 $F·g^{-1}$ at 1 $A·g^{-1}$ in 2 $mol·L^{-1}$ KOH aqueous electrolyte, as well as long cyclic stability with 94.5% maintained capacitance after 5000 cycles of charge–discharge at a current density 5 $A·g^{-1}$. The fabricated ASC using the $Ni_3S_4//CC$ as positive electrode and active carbon (AC) as negative electrode demonstrates an enlarged cell voltage to 1.5 V in polyvinyl alcohol–potassium hydroxide (PVA/KOH) electrolyte. The capacitance retention of ASC device is around 84.7% over 5000 cycles at the current density of 1 $A·g^{-1}$ along with a superior energy density (14.6 $W·kg^{-1}$ at a power density of 750.8 $W·kg^{-1}$) and high power density (6750 $W·kg^{-1}$ at an energy density of 5.4 $W·kg^{-1}$).

6.2 MoS_2/Ni_3S_4 composites

The incorporation of 2D MoS_2 with nickel sulfides could boost the synergetic effect and will be beneficial to further high-performance application [167–169]. Zhang et al. [164] designed $Ni_3S_4@MoS_2$ hierarchical nanostructures for SCs via a well-organized strategy to totally utilize the merits of each component. For the coated crystalline Ni_3S_4 core with the amorphous MoS_2 shell ($Ni_3S_4@MoS_2$) fabricated via a facile one-pot route, amorphous MoS_2 (indicating a specific capacitance of 1.6 times as that of the

crystalline counterpart) can raise the electrochemical performance of the electrode materials, achieving a superior specific capacitance of 1441 $F·g^{-1}$ at 2 $A·g^{-1}$. The core–shell structure showed 90.7% initial retention capacitance at 10 $A·g^{-1}$ over 3000 cycles and 76.2% maintained capacitance after 10,000 cycles. Luo et al. [110] constructed $Ni_3S_4–MoS_2$ heterojunction (Fig. 8a) electrode that displays a specific capacitance of 985 $F·g^{-1}$ at 1 $A·g^{-1}$ and 85% capacitance recovering (i.e., 573 $F·g^{-1}$) after 20,000 cycles at 10 $A·g^{-1}$ (Fig. 8b). The Ni_3S_4 support provides enhanced conductivity in the heterojunction and shows additional affinity with MoS_2, permitting a superior cycle life span. The $Ni_3S_4/MoS_2//AC$ (ASC) device demonstrates a high energy density of 58.43 $W·kg^{-1}$ when the power density extends 385.95 $W·kg^{-1}$ and retains an energy density of 18.75 $Wh·kg^{-1}$ even at a large power density of 7500 $W·kg^{-1}$. Huang et al. [136] synthesized $Ni_3S_4@MoS_2$ nanosheets decorated on carbon fiber paper ($Ni_3S_4@MoS_2/CFP$) by a facile one-step hydrothermal process. The $Ni_3S_4@MoS_2/CFP$ exhibits a remarkable specific capacitance (1296 $F·g^{-1}$), excellent rate capability and long cycling stability (96.2% retention over 5000 cycles at 5 $A·g^{-1}$). The $Ni_3S_4@MoS_2/CFP$ electrode delivers a high specific performance of 1296 $F·g^{-1}$ at 1 $A·g^{-1}$ in 2 $mol·L^{-1}$ KOH solution. Wang et al. [82] fabricated an advanced rose-like Ni_3S_4 microflower by a
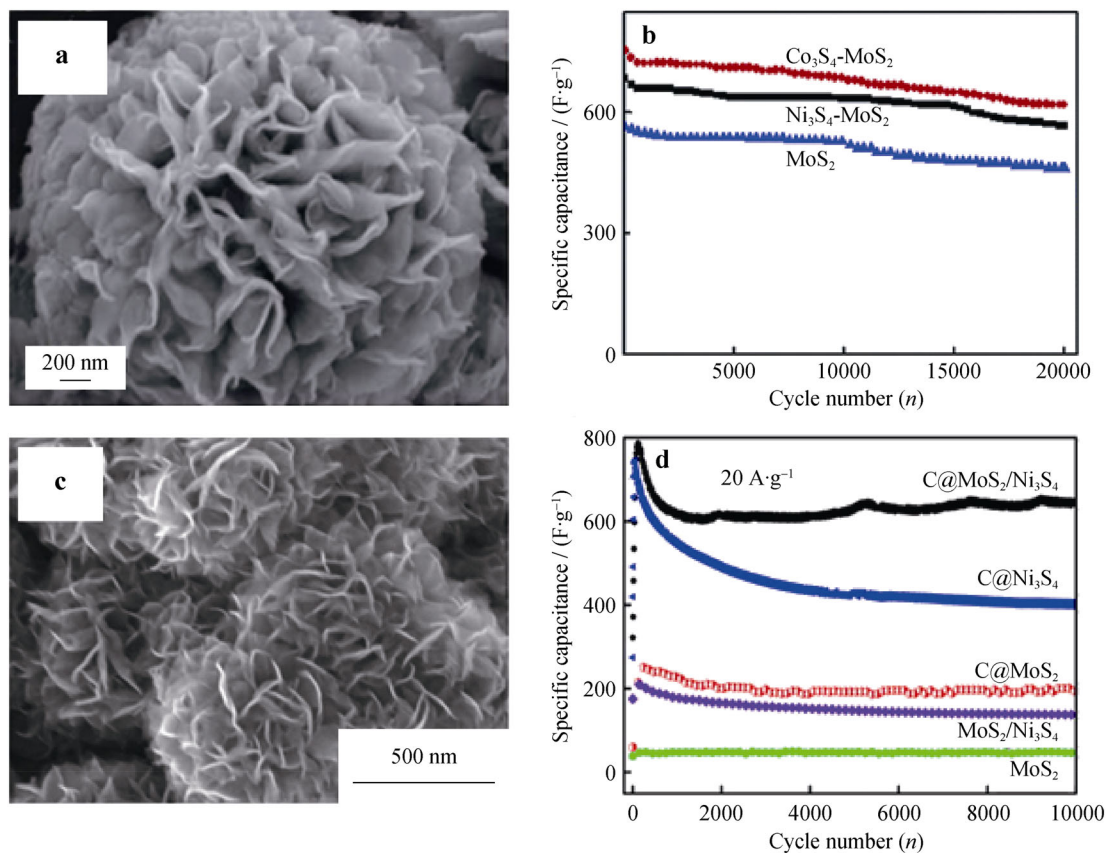
Fig. 8 a SEM image of Ni$_3$S$_4$–MoS$_2$; **b** cycling performances of MoS$_2$, Co$_3$S$_4$–MoS$_2$ and Ni$_3$S$_4$–MoS$_2$ at a current density of 10 A·g^{-1} (reproduced from Ref. [110], Copyright 2017 The Royal Society of Chemistry); **c** SEM image of C@MoS$_2$/Ni$_3$S$_4$ composite; **d** cycling performance of C@MoS$_2$/Ni$_3$S$_4$, C@Ni$_3$S$_4$, C@MoS$_2$, MoS$_2$/Ni$_3$S$_4$ and MoS$_2$ samples at 20 A·g^{-1}. (reproduced from Ref. [137], Copyright 2018 Elsevier)

direction exchange from the as-synthesized Ni(OH)$_2$ microflowers with sulfur based on the mechanism of self-assembly and oriented attachment crystal growth process under hydrothermal conditions [170]. The Ni$_3$S$_4$ microflower electrode displays a high specific capacitance of 1703 F·g^{-1} at 1 A·g^{-1} and even 1165 F·g^{-1} when the current density is raised to 10 A·g^{-1}. Furthermore, the Ni$_3$S$_4$//AC device exhibited superior cycling performance ($\sim$ 93% retained capacitance after 5000 cycles). To enhance the cycling stability of Ni$_3$S$_4$ at high current densities, an electrode of controlled MoS$_2$/Ni$_3$S$_4$ composite nanosheets wrapped on interconnected carbon shells (C@MoS$_2$/Ni$_3$S$_4$) was designed (Fig. 8c) [137] by a multistep process. The as-prepared composite reveals excellent cycling performance at large current densities due to its synergistic effects. After 10,000 cycles at 20 A·g^{-1} (Fig. 8d), a specific capacitance of 640.7 F·g^{-1}, even much larger than the starting value, can be displayed. Electrochemical tests demonstrate that the interconnected C shells can decrease the equivalent series resistance (ESR) and the incorporation of MoS$_2$ can exceptionally raise the cycling stability. In addition, the MoS$_2$/Ni$_3$S$_4$ nanosheets spread

around the C shells have greater contacts with the electrolyte and meanwhile buffer the volume change during the charge–discharge process.

6.3 Ni$_x$S$_y$/Ni$_3$S$_4$ composites

Apart from the hierarchical design and electronic conductivity, the reversible Faradaic reaction included in the charging/discharging process also has effect on the cycle performance [163, 171]. Transition-metal oxides or hydroxides of the similar metal but with double edges as hybrid supercapacitor electrode materials can assist in the cycling life [163, 171]. Moreover, morphology and composition are significant features for boosting the specific capacity, rate capability and cycling stability of electrode materials in electrochemical energy storage devices. With the beneficial particle size (200–400 nm) and composition, the NiS/Ni$_3$S$_4$ composite synthesized by Gou et al. [171] can deliver a favored gravimetric capacity (194.4 mAh·g^{-1} at 2 A·g^{-1}, and 133.1 mAh·g^{-1} at 10 A·g^{-1}) and enhanced cycling stability (89.5 mAh·g^{-1} at 10 A·g^{-1} after 5000 cycles). The nanoparticles inside could buffer the volume

changes during the long-term cycling, and for the pseudocapacitive mechanism, redox reaction is attributed to the reformation of Ni^{2+}/Ni^{3+} couple. And the synergistic effect is obtained from an intimate contact between NiS and Ni_3S_4, and the pinning/interaction of Ni_3S_4 with NiS could inhibit nickel sulfide particles from aggregating and avoid electrode material dissolution into the electrolyte. Cheng et al. [163] rationally designed and synthesized size-tunable hierarchical hollow core–shell submicrospheres based on nickel sulfide via a one-step hydrothermal process, in which Ni_3S_2/NiS hollow submicrosphere works as a core and Ni_3S_4 nanoflakes as shell. SEM and TEM images revealed the 3D hollow submicrospheres with lots of nanoflakes uniformly wrapped on the surface of hollow sphere with a diameter of 230 nm (Fig. 9a–c). The diameter of the hierarchical sphere can be managed by cetyltrimethylammonium bromide (CTAB). The unique structure design and mechanism is consistently investigated, and it can be assigned to a synergetic process of cage effect, Kirkendall effects and Ostwald ripening. When accommodated as electrodes for SCs, the optimized hybrids revealed a large specific capacity of 1031 $C\cdot g^{-1}$ (286.5 $mAh\cdot g^{-1}$) at a current density of 2 $A\cdot g^{-1}$. Even as the current density rises to 40 $A\cdot g^{-1}$, the hierarchical core–shell nanosphere still retains 614 $C\cdot g^{-1}$, showing an extraordinary rate capacity; it also exhibits a high retained capacitance of 90.3% after 3000 cycles at 10 $A\cdot g^{-1}$, due to the synergistic effects of multiphase nickel sulfides. Furthermore, the optimized ASC based on the Ni_3S_2/NiS@-Ni_3S_4 hierarchical hollow core–shell submicrospheres and rGO (NHS//rGO) shows good cycling stability (94.4% of the initial capacitance value after 14,000 cycles at 10 $A\cdot g^{-1}$), high power density and energy density (Fig. 9d, e).
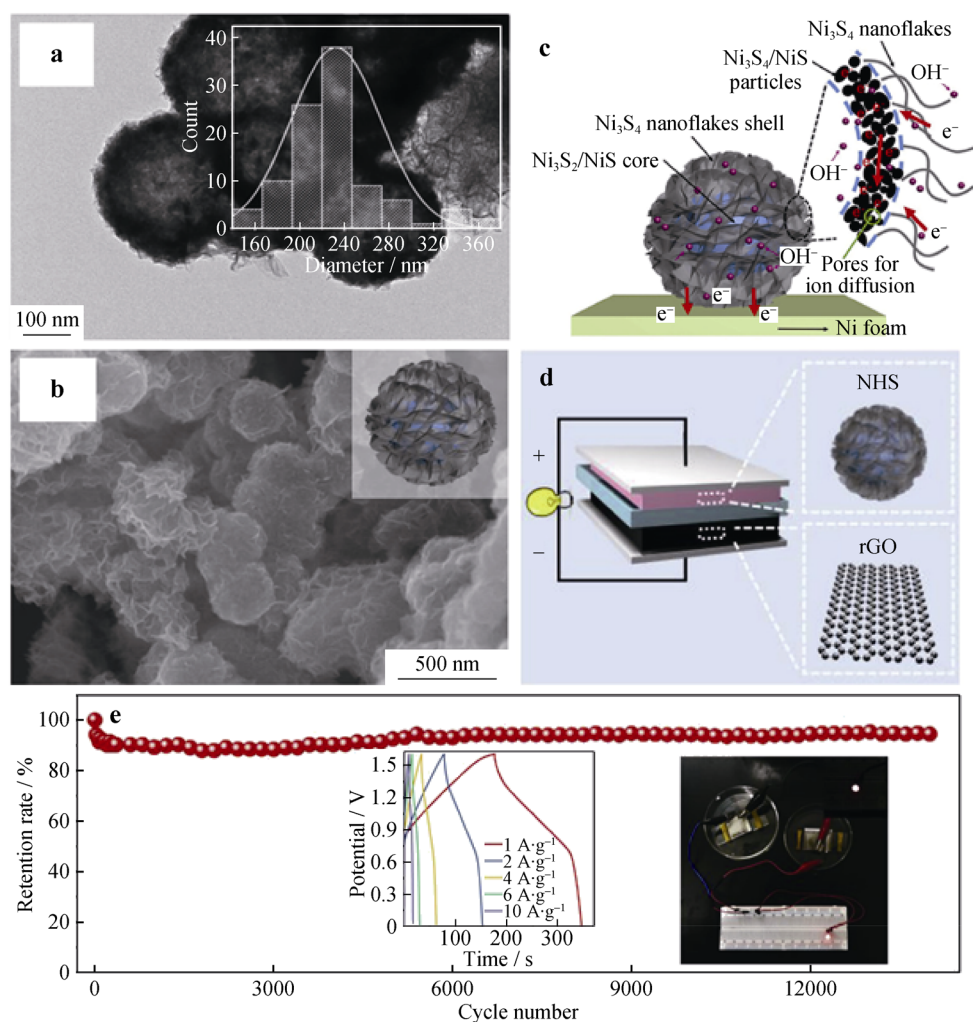
Fig. 9 **a** TEM image (inset being diameter distribution histogram) and **b** SEM image of Ni_3S_2/NiS@Ni_3S_4 core/shell hollow submicrospheres (NHS); **c** hybrid NHS-3 nanostructure diagram; **d** schematic illustration of NHS-3//rGO ASC device configuration, and **e** cycling stability of the ASC (insets being GCD curves of NHS-3//rGO ASC at different current densities and photograph showing that two SCs in series can light up a red LED). (reproduced from Ref. [163]. Copyright 2018 Elsevier)

Composition and morphology control of electrode materials is a successful route to boost the specific capacity, rate performance and cycling stability of electrochemical energy storage devices. Dai et al. [83] synthesized delicate nickel sulfide nanostructures as battery-type electrode for hybrid capacitor, where the phase structure and morphology are tuned by changing the initial $NiCl_2$/S mole ratio and hydrothermal synthesis conditions to produce a three-phase nickel sulfide (NiS–Ni_3S_2–Ni_3S_4, indicated as TP-Ni_xS_y) with 3D flower-like design made up of interconnected nanoflakes. The as-synthesized TP-Ni_xS_y shows a specific capacity of 724 C·g^{-1} at a current density of 1 A·g^{-1}. When incorporated with rGO, the TP-Ni_xS_y/rGO composite electrode demonstrates not only higher specific capacity (807 C·g^{-1} at 1 A·g^{-1}) but also better rate capability ($\sim$ 72% capacity recovered as the current density accumulated from 1 to 20 A·g^{-1}). Moreover, the hybrid capacitor, fabricated from a TP-Ni_xS_y/rGO positive electrode and a graphene-based negative electrode, exhibits a high energy density of 46 W·kg^{-1} at a power density of 1.8 kW·kg^{-1}, and retains an energy density of 32 W·kg^{-1} at a power density of 17.2 kW·kg^{-1}, signifying a promising potential for practical application.

7 Conclusion and perspectives

Supercapacitors are a prominent energy storage technology in developing the renewables and electric vehicles. Numerous synthetic approaches have been prospected to upgrade the electrochemical performance of electrode materials for SCs. Nickel sulfides and their hybrids are promising and competent candidates to alleviate the challenges for SCs because of their specific structure and properties.

We here propose some future perspectives of nickel sulfide-based materials for high-performance SCs listed as follows:

1. To enhance the performance of nickel sulfides through preparing the nanostructures with tunable morphologies that possess high surface area, good conductivity and appropriate pore properties. Nanostructures with large specific surface area will build effective contact between electrode and electrolyte ions, furnishing abundant electroactive sites for energy storage, specifically at high discharge currents.

2. To enhance the conductivity by constructing nanocomposites. Nickel sulfides/carbon composites not only illustrate the merits of the components but also conquer the defects of single constituents. The integration of nickel sulfides with carbon materials (e.g., graphene, carbon nanotubes and carbon nanofibers) can combine the advantages from all the constituents, and this strategy has been considered as one of the most prominent techniques to enhance the conductivity of nickel sulfide-based materials.

3. To obtain high energy density beyond high power density through fabricating a hybrid capacitor. As we know, the operational potential window of nickel sulfides is restricted by its intrinsic electrochemical properties. Integrating nickel sulfide materials as the cathode and carbon materials as the anode for hybrid capacitors will realize a larger potential window and higher energy/power densities thereof.

4. It is noteworthy that there is hardly any report on SCs with nickel sulfides electrodes based on organic electrolytes probably due to that the adoption of organic electrolytes in this kind of cell with nickel sulfides as cathode/positive electrode will not significantly extend the potential window but reduce the performance of SCs, especially power density due to lowered electrolyte conductivity. Moreover, as we know, in a related battery-type cell of NiS//Li, the discharge plateau is around 1.5 V using an organic electrolyte [172]; when the Li anode/negative electrode is replaced by a carbon electrode which is similar to the hybrid capacitor system, lithium plating may occur in an extended potential window and the rate/power-output performance may be a shortcoming. However, the adoption of some specific electrolytes such as redox-active electrolytes, water-in-salt electrolytes (including the saturated $NaClO_4$ aqueous electrolyte with a wide potential window over 3 V [173]) and ionic liquids could be a promising trend [174].

5. To design electrodes with enhanced structural and cyclic stability. It is of great importance to design and synthesize advanced electrodes and cells with cost-efficient strategies based on further insight into the electrochemical mechanism of nickel sulfides amid the large transition-metal chalcogenide family. Furthermore, avoiding the usage of inactive components such as binders, current collectors for self-supporting electrodes will also enhance the energy densities of devices.

References

[1] Xu BL, Qi SH, Jin MM, Cai XY, Lai LF, Sun ZT, Han XG, Lin ZF, Shao H, Peng P, Xiang ZH, Elshof JE, Tan R, Liu C, Zhang ZX, Duan XC, Ma JM. 2020 roadmap on two-dimensional materials for energy storage and conversion. Chin Chem Lett. 2019;30(12):2053.

[2] Pham TN, Park D, Lee Y, Kim IT, Hur J, Oh Y-K, Lee Y-C. Combination-based nanomaterial designs in single and double dimensions for improved electrodes in lithium ion-batteries and faradaic supercapacitors. J Energy Chem. 2019;38:119.

[3] Zhou XL, Liu QR, Jiang CL, Ji BF, Ji XL, Tang YB, Cheng HM. Strategies towards low-cost dual-ion batteries with high performance. Angew Chem In Ed. 2019;58:2.

[4] Jamesh M-I. Recent advances on flexible electrodes for Na-ion batteries and Li–S batteries. J. Energy Chem. 2019;32:15.

[5] Yang CS, Gao KN, Zhang XP, Sun Z, Zhang T. Rechargeable solid-state Li-air batteries: a status report. Rare Met. 2018;37(6):459.

[6] Xiao L, Li EW, Yi JY, Meng W, Deng BH, Liu JP. Enhanced performance of solid-state Li-O$_2$ battery using a novel integrated architecture of gel polymer electrolyte and nanoarray cathode. Rare Met. 2018;37(6):527.

[7] Liu Y, Yao MJ, Zhang LL, Niu ZQ. Large-scale fabrication of reduced graphene oxide-sulfur composite films for flexible lithium-sulfur batteries. J Energy Chem. 2019;38:199.

[8] Li F, Liu QH, Hu JW, Feng YZ, He PB, Ma JM. Recent advances in cathode materials for rechargeable lithium–sulfur batteries. Nanoscale. 2019;11(33):15418.

[9] Ma W, Xu Q. Lithium cobaltate: a novel host material enables high-rate and stable lithium–sulfur batteries. Rare Met. 2018;37(11):929.

[10] Lu H, Chen Z, Du HL, Zhang K, Wang JL, Hou ZZ, Fang J. The enhanced performance of lithium sulfur battery with ionic liquid-based electrolyte mixed with fluorinated ether. Ionics (Kiel). 2019;25(6):2685.

[11] Shen X, Cheng XB, Shi P, Huang JQ, Zhang XQ, Yan C, Li T, Zhang Q. Lithium–matrix composite anode protected by a solid electrolyte layer for stable lithium metal batteries. J Energy Chem. 2019;37:29.

[12] Wu DX, Wang CY, Wu MG, Chao YF, He PB, Ma JM. Porous bowl-shaped VS$_2$ nanosheets/graphene composite for high-rate lithium-ion storage. J Energy Chem. 2020;43:24.

[13] Yan ZH, Yang QW, Wang QH, Ma JM. Nitrogen doped porous carbon as excellent dual anodes for Li- and Na-ion batteries. Chin Chem Lett. 2020;31(2):583.

[14] Li HJ, Lu M, Han WJ, Li HB, Wu YC, Zhang W, Wang JC, Zhang BS. Employing MXene as a matrix for loading amorphous Si generated upon lithiation towards enhanced lithium-ion storage. J Energy Chem. 2019;32:15.

[15] Dong Y, Feng YZ, Deng JW, He PB, Ma JM. Electrospun Sb$_2$Se$_3$@C nanofibers with excellent lithium storage properties. Chin Chem Lett. 2020;31(3):909.

[16] Yuan CF, Wu C, Zhang Z, Hu GR. Evaluation of LiMn$_2$O$_4$--LiNi$_{0.8}$0Co$_{0.15}$Al$_{0.05}$O$_2$ hybrid material as cathode in soft-packed lithium ion battery. Ionics (Kiel). 2017;23(3):567.

[17] Qi SH, Xu BL, Tiong VT, Hu J, Ma JM. Progress on iron oxides and chalcogenides as anodes for sodium-ion batteries. Chem Eng J. 2020;379:122261.

[18] Cheng DL, Yang LC, Zhu M. High-performance anode materials for Na-ion batteries. Rare Met. 2018;37(3):167.

[19] Xu BL, Qi SH, He PB, Ma JM. Antimony- and bismuth- based chalcogenides for sodium-ion batteries. Chem Asian J. 2019;14(17):2925.

[20] Etman AS, Sun JL, Younesi R. V$_2$O$_5$·nH$_2$O nanosheets and multi-walled carbon nanotube composite as a negative electrode for sodium-ion batteries. J Energy Chem. 2019;30:145.

[21] Hou HS, Banks CE, Jing MJ, Zhang Y, Ji XB. Carbon quantum dots and their derivative 3D porous carbon frameworks for sodium-ion batteries with ultralong cycle life. Adv Mater. 2015;27(47):7861.

[22] Xie DH, Zhang M, Wu Y, Xiang L, Tang YB. A Flexible dual-ion battery based on sodium-ion quasi-solid-state electrolyte with long cycling life. Adv Funct Mater. 2020;30(5):1906770.

[23] Cai YS, Fang GZ, Zhou J, Liu SN, Luo ZG, Pan AQ, Cao GZ, Liang SQ. Metal-organic framework-derived porous shuttle-like vanadium oxides for sodium-ion battery application. Nano Res. 2018;11(1):449.

[24] Wu D, Zhang W, Feng Y, Ma J. Necklace-like carbon nanofibers encapsulating V$_3$S$_4$ microspheres for ultrafast and stable potassium-ion storage. J Mater Chem A. 2020;8:2618.

[25] Xu BL, Qi SH, Li F, Peng XX, Cai JF, Liang JJ, Ma JM. Cotton-derived oxygen/sulfur co-doped hard carbon as advanced anode material for potassium-ion batteries. Chin Chem Lett. 2019;31(1):217.

[26] Xie X, Qi SH, Wu DX, Wang HP, Li F, Peng XX, Cai JF, Liang JJ, Ma JM. Porous surfur-doped hard carbon for excellent potassium storage. Chin Chem Lett. 2020;31(1):223.

[27] Qi SH, Xie X, Peng XW, Ng DHL, Wu MG, Liu QH, Yang JL, Ma JM. Mesoporous carbon-coated bismuth nanorods as anode for potassium-ion batteries. Phys Status Solidi RRL. 2019;13(10):1900209.

[28] Chang XQ, Zhou XL, Ou XW, Lee CS, Zhou JW, Tang YB. Ultrahigh nitrogen doping of carbon nanosheets for high capacity and long cycling potassium ion storage. Adv Energy Mater. 2019;9(47):1902672.

[29] Xia C, Guo J, Lei YJ, Liang HF, Zhao C, Alshareef HN. Rechargeable aqueous zinc-ion battery based on porous framework zinc pyrovanadate intercalation cathode. Adv Mater. 2018;30(5):1705580.

[30] Mo FN, Liang GJ, Meng QQ, Liu ZX, Li HF, Fan J, Zhi CY. A flexible rechargeable aqueous zinc manganese-dioxide battery working at − 20 °C. Energy Environ Sci. 2019;12(2):706.

[31] Su CY, Cheng H, Li W, Liu ZQ, Li N, Hou ZF, Bai FQ, Zhang HX, Ma TY. Atomic modulation of FeCo-nitrogen-carbon bifunctional oxygen electrodes for rechargeable and flexible all-solid-state zinc-air battery. Adv Energy Mater. 2017;7(13):1602420.

[32] Zhang ZJ, Zhou DB, Zhou L, Yu HZ, Huang BY. NiFe LDH-CoPc/CNTs as novel bifunctional electrocatalyst complex for zinc–air battery. Ionics (Kiel). 2018;24(6):1709.

[33] Wu MG, Xu BL, Zhang YF, Qi SH, Ni W, Hu J, Ma JM. Perspectives in emerging bismuth electrochemistry. Chem Eng J. 2020;381:122558.

[34] Liao JQ, Ni W, Wang CY, Ma JM. Layer-structured niobium oxides and their analogues for advanced hybrid capacitors. Chem Eng J. 2020;391:123489.

[35] Zhang D, Wang H, Chen G, Wan H, Zhang N, Liu XH, Ma RZ. Post-synthesis isomorphous substitution of layered Co–Mn hydroxide nanocones with graphene oxide as high-performance supercapacitor electrodes. Nanoscale. 2019;11(13):6165.

[36] Li HY, Guo H, Tong SC, Huang KQ, Zhang CJ, Wang XF, Zhang D, Chen XH, Yang JL. High-performance supercapacitor carbon electrode fabricated by large-scale roll-to-roll micro-gravure printing. J Phys D Appl Phys. 2019;52(11):115501.

[37] Winter M, Brodd RJ. What are batteries, fuel cells, and supercapacitors? Chem Rev. 2004;104(10):4245.

[38] Arbizzani C, Yu Y, Li J, Xiao J, Xia YY, Yang Y, Santato C, Raccichini R, Passerini S. Good practice guide for papers on supercapacitors and related hybrid capacitors for the Journal of Power Sources. J Power Sources. 2020;450:227636.

[39] Chhowalla M, Shin HS, Eda G, Li L, Loh KP, Zhang H. The chemistry of two-dimensional layered transition metal dichalcogenide nanosheets. Nat Chem. 2013;5(4):263.

[40] Zhu YW, Murali S, Stoller MD, Ganesh KJ, Cai W, Paulo JF, Adam P, Robert MW, Katie AC, Matthias T, Dong S, Eric AS, Rodney SR. Carbon-based supercapacitors produced by activation of graphene. Science. 2011;332(6037):1537.

[41] Tie D, Huang SF, Wang J, Ma J, Zhang JJ, Zhao YF. Hybrid energy storage devices: advanced electrode materials and matching principles. Energy Storage Mater. 2019;21:22.

[42] Wu MG, Ni W, Hu J, Ma JM. NASICON-structured NaTi$_2$(PO$_4$)$_3$ for sustainable energy storage. Nano-Micro Lett. 2019;11(1):44.

[43] Wang L, Xie X, Dinh KN, Yan QY, Ma JM. Synthesis, characterizations, and utilization of oxygen-deficient metal oxides for lithium/sodium-ion batteries and supercapacitors. Coord Chem Rev. 2019;397:138.

[44] Kang B, Ceder G. Battery materials for ultrafast charging and discharging. Nature. 2009;458(7235):190.

[45] De Volder MFL, Tawfick SH, Baughman RH, Hart AJ. Carbon nanotubes: present and future commercial applications. Science. 2013;339(6119):535.

[46] Simon P, Gogotsi Y, Dunn B. Where do batteries end and supercapacitors begin? Science. 2014;343(6176):1210.

[47] Yan J, Wang Q, Wei T, Fan ZG. Recent advances in design and fabrication of electrochemical supercapacitors with high energy densities. Adv Energy Mater. 2014;4(4):1300816.

[48] Wang F, Wu X, Yuan X, Liu ZC, Zhang Y, Fu LJ, Zhu YS, Zhou QM, Wu YP, Huang W. Latest advances in supercapacitors: from new electrode materials to novel device designs. Chem Soc Rev. 2017;46(22):6816.

[49] Li Q, Zheng SS, Xu YX, Xue HG, Pang H. Ruthenium based materials as electrode materials for supercapacitors. Chem Eng J. 2018;333:505.

[50] Borenstein A, Hanna O, Attias R, Luski S, Brousse T, Aurbach D. Carbon-based composite materials for supercapacitor electrodes: a review. J Mater Chem A. 2017;5(25):12653.

[51] Feng DW, Lei T, Lukatskaya MR, Park JH, Huang ZH, Lee M, Shaw L, Chen SC, Yakovenko AA, Kulkarni A, Xiao JP, Fredrickson K, Tok JB, Zou XD, Bao ZN. Robust and conductive two-dimensional metal–organic frameworks with exceptionally high volumetric and areal capacitance. Nat Energy. 2018;3(1):30.

[52] Zuo WH, Li RZ, Zhou C, Li YY, Xia JL, Liu JP. Battery-supercapacitor hybrid devices: recent progress and future prospects. Adv Sci. 2017;4(7):1600539.

[53] Tan CL, Cao XH, Wu XJ, He QY, Yang J, Zhang X, Chen JZ, Zhao W, Han SK, Nam GH, Sindoro M, Zhang H. Recent advances in ultrathin two-dimensional nanomaterials. Chem Rev. 2017;117(9):6225.

[54] Shao YL, El-Kady MF, Sun JY, Li YG, Zhang QH, Zhu MF, Wang HZ, Dunn B, Kaner RB. Design and mechanisms of asymmetric supercapacitors. Chem Rev. 2018;118(18):9233.

[55] Yuan CZ, Wu HB, Xie Y, Lou XW. Mixed transition-metal oxides: design, synthesis, and energy-related applications. Angew Chem In Ed. 2014;53(6):1488.

[56] Faraji S, Ani FN. Microwave-assisted synthesis of metal oxide/hydroxide composite electrodes for high power supercapacitors—a review. J Power Sources. 2014;263:338.

[57] Cheng JP, Zhang J, Liu F. Recent development of metal hydroxides as electrode material of electrochemical capacitors. RSC Adv. 2014;4(73):38893.

[58] Yu XY, Lou XW. Mixed metal sulfides for electrochemical energy storage and conversion. Adv Energy Mater. 2018;8(3):1701592.

[59] Chandrasekaran S, Yao LB, Deng LB, Bowen C, Zhang Y, Chen SM, Lin ZQ, Peng F, Zhang PX. Recent advances in metal sulfides: from controlled fabrication to electrocatalytic, photocatalytic and photoelectrochemical water splitting and beyond. Chem Soc Rev. 2019;48(15):4178.

[60] Deng XL, Jiang YQ, Wei ZX, Mao ML, Pothu R, Wang HX, Wang CY, Liu JP, Ma JM. Flexible quasi-solid-state dual-ion asymmetric supercapacitor based on Ni(OH)$_2$ and Nb$_2$O$_5$ nanosheet arrays. Green Energy Environ. 2019;4(4):382.

[61] Fong KD, Wang T, Smoukov SK. Multidimensional performance optimization of conducting polymer-based supercapacitor electrodes. Sustain Energy Fuels. 2017;1(9):1857.

[62] Rajender B, Palaniappan S. Simultaneous oxidation and doping of aniline to polyaniline by oxidative template: electrochemical performance in supercapacitor. Int J Polym Mater Polym Biomater. 2015;64(18):939.

[63] Boddula R, Srinivasan P. Role of dual dopants in highly ordered crystalline polyaniline nanospheres: electrode materials in supercapacitors. J Appl Polym Sci. 2015;132(36):42510.

[64] Bolagam R, Boddula R, Srinivasan P. Synthesis of highly crystalline polyaniline with the use of (cyclohexylamino)-1-propanesulfonic acid for supercapacitor. J Appl Electrochem. 2015;45(1):51.

[65] Rajender B, Palaniappan S. Organic solvent soluble methyltriphenylphosphonium peroxodisulfate: a novel oxidant for the synthesis of polyaniline and the thus prepared polyaniline in high performance supercapacitors. New J Chem. 2015;39(7):5382.

[66] He JP, Guo C, Zhou SW, Zhao YL, Wang QP, Yang S, Yang JQ, Wang QH. Dual carbon-modified nickel sulfide composites toward high-performance electrodes for supercapacitors. Inorg Chem Front. 2018;6(1):226.

[67] Wang QH, Zhu YX, Xue J, Zhao XS, Guo ZP, Wang C. General synthesis of porous mixed metal oxide hollow spheres with enhanced supercapacitive properties. ACS Appl Mater Interfaces. 2016;8(27):17226.

[68] Wang QH, Du JL, Zhu YX, Yang JQ, Chen J, Wang C, Li L, Jiao LF. Facile fabrication and supercapacitive properties of mesoporous zinc cobaltite microspheres. J Power Sources. 2015;284:138.

[69] Wang QH, Zhu LX, Sun LQ, Liu YC, Jiao LF. Facile synthesis of hierarchical porous ZnCo$_2$O$_4$ microspheres for high-performance supercapacitors. J Mater Chem A. 2015;3(3):982.

[70] Rui XH, Tan HT, Yan QY. Nanostructured metal sulfides for energy storage. Nanoscale. 2014;6(17):9889.

[71] Kulkarni P, Nataraj SK, Balakrishna RG, Nagaraju DH, Reddy MV. Nanostructured binary and ternary metal sulfides: synthesis methods and their application in energy conversion and storage devices. J Mater Chem A. 2017;5(42):22040.

[72] Wang QH, Jiao LF, Du HM, Si YC, Wang YJ, Yuan HT. Co$_3$S$_4$ hollow nanospheres grown on graphene as advanced electrode materials for supercapacitors. J Mater Chem. 2012;22(40):21387.

[73] Wang QH, Jiao LF, Du HM, Si YC, Wang YJ, Yuan HT. Facile synthesis and superior supercapacitor performances of three-dimensional cobalt sulfide hierarchitectures. CrystEngComm. 2011;13(23):6960.

[74] Wen XR, Zhao MQ, Zhang M, Fan X, Zhang DS. Efficient capacitive deionization of saline water by an integrated tin disulfide nanosheet@graphite paper electrode via an in situ growth strategy. ACS Sustain Chem Eng. 2020;8(2):1268.

[75] Han JL, Yan TT, Shen JJ, Shi LY, Zhang JP, Zhang DS. Capacitive deionization of saline water by using

MoS$_2$–graphene hybrid electrodes with high volumetric adsorption capacity. Environ Sci Technol. 2019;53(21):12668.

[76] Wang PT, Zhang X, Zhang J, Wan S, Guo SJ, Lu G, Yao JL, Huang XQ. Precise tuning in platinum-nickel/nickel sulfide interface nanowires for synergistic hydrogen evolution catalysis. Nat Commun. 2017;8:14580.

[77] Ye C, Zhang L, Guo CX, Li DD, Vasileff A, Wang HH, Qiao SZ. A 3D Hybrid of chemically coupled nickel sulfide and hollow carbon spheres for high performance lithium-sulfur batteries. Adv Funct Mater. 2017;27(33):1702524.

[78] Sun HC, Qin D, Huang SQ, Guo XZ, Li DM, Luo YH, Meng QB. Dye-sensitized solar cells with NiS counter electrodes electrodeposited by a potential reversal technique. Energy Environ Sci. 2011;4(8):2630.

[79] Zhao J, Li ZJ, Yuan XC, Shen T, Lin LG, Zhang M, Meng A, Li QD. Novel core-shell multi-dimensional hybrid nanoarchitectures consisting of Co(OH)$_2$ nanoparticles/Ni$_3$S$_2$ nanosheets grown on SiC nanowire networks for high-performance asymmetric supercapacitors. Chem Eng J. 2019;357:21.

[80] Chen FS, Wang H, Ji S, Linkov V, Wang RF. Core-shell structured Ni$_3$S$_2$@Co(OH)$_2$ nano-wires grown on Ni foam as binder-free electrode for asymmetric supercapacitors. Chem Eng J. 2018;345:48.

[81] Lin JH, Zheng XH, Wang YH, Liang HY, Jia HN, Qi JL, Cao J, Fei WD, Feng JC. Rational construction of core-shell Ni$_3$S$_2$@Ni(OH)$_2$ nanostructures as battery-like electrodes for supercapacitors. Inorg Chem Front. 2018;5(8):1985.

[82] Wang HY, Liang MM, Duan D, Shi WY, Song YY, Sun ZB. Rose-like Ni$_3$S$_4$ as battery-type electrode for hybrid supercapacitor with excellent charge storage performance. Chem Eng J. 2018;350:523.

[83] Dai SG, Zhao BT, Qu C, Chen DC, Dang D, Song B, deGlee BM, Fu JW, Hu CG, Wong CP, Liu ML. Controlled synthesis of three-phase Ni$_x$S$_y$/rGO nanoflake electrodes for hybrid supercapacitors with high energy and power density. Nano Energy. 2017;33:522.

[84] Li YH, Cao LJ, Qiao LQ, Zhou M, Xiao P, Zhang YH. Ni-Co sulfide nanowires on nickel foam with ultrahigh capacitance for asymmetric supercapacitors. J Mater Chem A. 2014;2(18):6540.

[85] Naveenkumar P, Paruthimal Kalaignan G. Electrodeposited MnS on graphene wrapped Ni-Foam for enhanced supercapacitor applications. Electrochim Acta. 2018;289:437.

[86] Xing JL, Du J, Zhang X, Shao YB, Zhang T, Xu CL. A Ni-P@NiCo LDH core–shell nanorod-decorated nickel foam with enhanced areal specific capacitance for high-performance supercapacitors. Dalt Trans. 2017;46(30):10064.

[87] Sun HH, Ma Z, Qiu YF, Liu H, Gao GG. Ni@NiO nanowires on nickel foam prepared via "acid hungry" strategy: high supercapacitor performance and robust electrocatalysts for water splitting reaction. Small. 2018;14(31):1800294.

[88] He Y, Zhuang X, Lei C, Lei L, Hou Y, Mai Y, Feng X. Porous carbon nanosheets: synthetic strategies and electrochemical energy related applications. Nano Today. 2019;24:103.

[89] Huang JQ, Wang ZY, Xu ZL, Chong XW, Qin XY, Wang XY, Kim JK. Three-dimensional porous graphene aerogel cathode with high sulfur loading and embedded TiO$_2$ nanoparticles for advanced lithium-sulfur batteries. ACS Appl Mater Interfaces. 2016;8(42):28663.

[90] Ding YB, Tang YH, Yang LM, Zeng YX, Yuan JL, Liu T, Zhang SQ, Liu CB, Luo SG. Porous nitrogen-rich carbon materials from carbon self-repairing g-C$_3$N$_4$ assembled with graphene for high-performance supercapacitor. J Mater Chem A. 2016;4(37):14307.

[91] Zhang W, Jin XZ, Chai H, Diao GW, Piao YZ. 3D hybrids of interconnected porous carbon nanosheets/vertically aligned polyaniline nanowires for high-performance supercapacitors. Adv Mater Interfaces. 2018;5(11):1800106.

[92] Hooch Antink W, Choi Y, Seong KD, Kim JM, Piao Y. Recent progress in porous graphene and reduced graphene oxide-based nanomaterials for electrochemical energy storage devices. Adv Mater Interfaces. 2018;5(5):1701212.

[93] Chao YZ, Chen SB, Chen HQ, Hu XJ, Ma Y, Guo WS, Bai YX. Densely packed porous graphene film for high volumetric performance supercapacitor. Electrochim Acta. 2018;276:118.

[94] Kang Z, Li Y, Yu YS, Liao QL, Zhang Z, Guo HJ, Zhang SC, Wu J, Si HN, Zhang XM, Zhang Y. Facile synthesis of NiCo$_2$S$_4$ nanowire arrays on 3D graphene foam for high-performance electrochemical capacitors application. J Mater Sci. 2018;53(14):10292.

[95] Wang HF, Tang C, Wang B, Li BQ, Cui X, Zhang Q. Defect-rich carbon fiber electrocatalysts with porous graphene skin for flexible solid-state zinc–air batteries. Energy Storage Mater. 2018;15:124.

[96] Shen F, Pankratov D, Chi QJ. Graphene-conducting polymer nanocomposites for enhancing electrochemical capacitive energy storage. Curr Opin Electrochem. 2017;4(1):133.

[97] Liu SH, Gordiichuk P, Wu ZS, Liu ZY, Wei W, Wagner M, Mohamed-Noriega N, Wu DQ, Mai YY, Herrmann A, Mullen K, Feng XL. Patterning two-dimensional free-standing surfaces with mesoporous conducting polymers. Nat Commun. 2015;6:8817.

[98] Zhao DP, Liu HQ, Wu X. Bi-interface induced multi-active MCo$_2$O$_4$@MCo$_2$S$_4$@PPy (M = Ni, Zn) sandwich structure for energy storage and electrocatalysis. Nano Energy. 2019;57:363.

[99] Fan ZM, Zhu JP, Sun XH, Cheng ZJ, Liu YY, Wang YS. High density of free-standing holey graphene/PPy films for superior volumetric capacitance of supercapacitors. ACS Appl Mater Interfaces. 2017;9(26):21763.

[100] Sajedi-Moghaddam A, Mayorga-Martinez CC, Sofer Z, Bouša D, Saievar-Iranizad E, Pumera M. Black phosphorus nanoflakes/polyaniline hybrid material for high-performance pseudocapacitors. J Phys Chem C. 2017;121(37):20532.

[101] Yu HT, Xin GX, Ge X, Bulin C, Li RH, Xing RG, Zhang BW. Porous graphene-polyaniline nanoarrays composite with enhanced interface bonding and electrochemical performance. Compos Sci Technol. 2018;154:76.

[102] Feng LD, Zhu YF, Ding HY, Ni CY. Recent progress in nickel based materials for high performance pseudocapacitor electrodes. J Power Sources. 2014;267:430.

[103] Ye L, Zhao LJ, Zhang H, Pan Z, Gen S, Shi WH, Han B, Sun HM, Yang XJ, Xu TH. Serpent-cactus-like Co-doped Ni(OH)$_2$/Ni$_3$S$_2$ hierarchical structure composed of ultrathin nanosheets for use in efficient asymmetric supercapacitors. J Mater Chem A. 2017;5(4):1603.

[104] Wen J, Li SZ, Chen T, Yue Y, Liu NS, Gao YH, Li B, Song ZC, Chen Z, Guo YX, Xiong R, Fang GJ. Three-dimensional hierarchical NiCo hydroxide@Ni$_3$S$_2$ nanorod hybrid structure as high performance positive material for asymmetric supercapacitor. Electrochim Acta. 2016;222:965.

[105] Yang X, Zhao L, Lian J. Arrays of hierarchical nickel sulfides/MoS$_2$ nanosheets supported on carbon nanotubes backbone as advanced anode materials for asymmetric supercapacitor. J Power Sources. 2017;343:373.

[106] Sun CC, Ma MZ, Yang J, Zhang YF, Chen P, Huang W, Dong XC. Phase-controlled synthesis of α-NiS nanoparticles confined in carbon nanorods for high performance supercapacitors. Sci Rep. 2015;4(1):7054.

[107] Harish S, Naveen AN, Abinaya R, Archana J, Ramesh R, Navaneethan M, Shimoura M, Hayakawa Y. Enhanced performance on capacity retention of hierarchical NiS hexagonal

nanoplate for highly stable asymmetric supercapacitor. Electrochim Acta. 2018;283:1053.

[108] Hou LR, Yuan CZ, Li DK, Yang L, Shen LF, Zhang F, Zhang XG. Electrochemically induced transformation of NiS nanoparticles into Ni(OH)₂ in KOH aqueous solution toward electrochemical capacitors. Electrochim Acta. 2011;56(22):7454.

[109] Qu C, Zhang L, Meng W, Liang ZB, Dang D, Dai SG, Zhao BT, Tabassum H, Gao S, Zhang H, Guo WH, Zhao R, Huang XY, Liu ML, Zou RQ. MOF-derived α-NiS nanorods on graphene as an electrode for high-energy-density supercapacitors. J Mater Chem A. 2018;6(9):4003.

[110] Luo WH, Zhang GF, Cui YX, Sun Y, Zhang J, Zheng WJ. One-step extended strategy for the ionic liquid-assisted synthesis of Ni₃S₄–MoS₂ heterojunction electrodes for supercapacitors. J Mater Chem A. 2017;5(22):11278.

[111] Xu YL, Du WM, Du LL, Zhu WJ, Guo W, Chang JJ, Zhang B, Deng DH. Monocrystalline NiS nanowire arrays supported by Ni foam as binder-free electrodes with outstanding performances. RSC Adv. 2017;7(36):22553.

[112] Chen ZH, Zhao MG, Lv X, Zhou K, Jiang XQ, Ren XL, Mei XF. Fast ion transport through ultrathin shells of metal sulfide hollow nanocolloids used for high-performance energy storage. Sci Rep. 2018;8(1):30.

[113] Wang J, Ma KY, Zhang J, Liu F, Cheng JP. Template-free synthesis of hierarchical hollow NiS$_x$ microspheres for supercapacitor. J Colloid Interface Sci. 2017;507:290.

[114] Patil AM, Lokhande AC, Chodankar NR, Kumbhar VS, Lokhande CD. Engineered morphologies of β-NiS thin films via anionic exchange process and their supercapacitive performance. Mater Des. 2016;97:407.

[115] Yu XY, Yu L, Wu HB, Lou XW. Formation of nickel sulfide nanoframes from metal-organic frameworks with enhanced pseudocapacitive and electrocatalytic properties. Angew Chem In Ed. 2015;54(18):5331.

[116] You B, Sun YJ. Hierarchically porous nickel sulfide multifunctional superstructures. Adv Energy Mater. 2016;6(7):1502333.

[117] Guan B, Li Y, Yin BY, Wang DW, Zhang HH, Cheng CJ. Synthesis of hierarchical NiS microflowers for high performance asymmetric supercapacitor. Chem Eng J. 2017;308:1165.

[118] Surendran S, Selvan RK. Growth and characterization of 3D flower-like β-NiS on carbon cloth: a dexterous and flexible multifunctional electrode for supercapattery and water-splitting applications. Adv Mater Interfaces. 2018;5(4):1701056.

[119] Du NX, Zheng WJ, Li XC, He HG, Wang L, Shi JH. Nanosheet-assembled NiS hollow structures with double shells and controlled shapes for high-performance supercapacitors. Chem Eng J. 2017;323:415.

[120] Yang JQ, Guo W, Li D, Wei HM, Wu LY, Zheng WJ. Synthesis and electrochemical performances of novel hierarchical flower-like nickel sulfide with tunable number of composed nanoplates. J Power Sources. 2014;268:113.

[121] Wang XH, Xia HY, Wang XQ, Shi B, Fang Y. A super high performance asymmetric supercapacitor based on Co₃S₄/NiS nanoplates electrodes. RSC Adv. 2016;6(100):97482.

[122] Theerthagiri J, Karuppasamy K, Durai G, Arunachalam P, Sangeetha K, Kuppusami P, Kim HS. Recent advances in metal chalcogenides (MX; X = S, Se) nanostructures for electrochemical supercapacitor applications: a brief review. Nanomaterials. 2018;8(4):256.

[123] AbdelHamid AA, Yang X, Yang J, Chen X, Ying JY. Graphene-wrapped nickel sulfide nanoprisms with improved performance for Li-ion battery anodes and supercapacitors. Nano Energy. 2016;26:425.

[124] Singh A, Roberts AJ, Slade RCT, Chandra A. High electrochemical performance in asymmetric supercapacitors using MWCNT/nickel sulfide composite and graphene nanoplatelets as electrodes. J Mater Chem A. 2014;2(39):16723.

[125] Liu T, Jiang CJ, Cheng B, You W, Yu JG. Hierarchical NiS/N-doped carbon composite hollow spheres with excellent supercapacitor performance. J Mater Chem A. 2017;5(40):21257.

[126] Xia W, Qu C, Liang ZB, Zhao BT, Dai SG, Qiu B, Jiao Y, Zhang QB, Huang XY, Guo WH, Dang D, Zou RQ, Xia DG, Liu ML. High-performance energy storage and conversion materials derived from a single metal-organic framework/graphene aerogel composite. Nano Lett. 2017;17(5):2788.

[127] Bendi R, Kumar V, Bhavanasi V, Parida K, Lee PS. Metal organic framework-derived metal phosphates as electrode materials for supercapacitors. Adv Energy Mater. 2016;6(3):1501833.

[128] Li Y, Ye K, Cheng K, Yin JL, Cao DX, Wang GL. Electrodeposition of nickel sulfide on graphene-covered make-up cotton as a flexible electrode material for high-performance supercapacitors. J Power Sources. 2015;274:943.

[129] Zhang YF, Zuo LZ, Zhang LS, Yan JL, Lu HY, Fan W, Liu TX. Immobilization of NiS nanoparticles on N-doped carbon fiber aerogels as advanced electrode materials for supercapacitors. Nano Res. 2016;9(9):2747.

[130] Lu M, Yuan XP, Guan XH, Wang GS. Synthesis of nickel chalcogenide hollow spheres using an L-cysteine-assisted hydrothermal process for efficient supercapacitor electrodes. J Mater Chem A. 2017;5(7):3621.

[131] Pi WB, Mei T, Li J, Wang JY, Li JH, Wang XB. Durian-like NiS₂@rGO nanocomposites and their enhanced rate performance. Chem Eng J. 2018;335:275.

[132] Xie SL, Gou JX, Liu B, Liu CG. Synthesis of cobalt-doped nickel sulfide nanomaterials with rich edge sites as high-performance supercapacitor electrode materials. Inorg Chem Front. 2018;5(5):1218.

[133] Sun HH, Wang JG, Zhang XZ, Li CJ, Liu F, Zhu WJ, Li YY, Shao MH. Nanoconfined construction of MoS₂@C/MoS₂ core–sheath nanowires for superior rate and durable Li-ion energy storage. ACS Sustain Chem Eng. 2019;7(5):5346.

[134] Ruan YJ, Jiang JJ, Wan HZ, Ji X, Miao L, Peng L, Zhang B, Lv L, Liu J. Rapid self-assembly of porous square rod-like nickel persulfide via a facile solution method for high-performance supercapacitors. J Power Sources. 2016;301:122.

[135] Ni W, Wang B, Cheng JL, Li XD, Guan Q, Gu GF, Huang L. Hierarchical foam of exposed ultrathin nickel nanosheets supported on chainlike Ni-nanowires and the derivative chalcogenide for enhanced pseudocapacitance. Nanoscale. 2014;6(5):2618.

[136] Huang F, Yan AH, Sui YW, Qi JQ, Meng QK, He YZ. One-step hydrothermal synthesis of Ni₃S₄@MoS₂ nanosheet on carbon fiber paper as a binder-free anode for supercapacitor. J Mater Sci: Mater Electron. 2017;28(17):12747.

[137] Qin SC, Yao TH, Guo X, Chen Q, Liu DQ, Liu QM, Li YL, Li JS, He DY. MoS₂/Ni₃S₄ composite nanosheets on interconnected carbon shells as an excellent supercapacitor electrode architecture for long term cycling at high current densities. Appl Surf Sci. 2018;440:741.

[138] Gou J. Ni₂P/NiS₂ composite with phase boundaries as high-performance electrode material for supercapacitor. J Electrochem Soc. 2017;164(13):A2956.

[139] Li XF, Shen JF, Li N, Ye MX. Template-free solvothermal synthesis of NiS₂ microspheres on graphene sheets for high-performance supercapacitors. Mater Lett. 2015;139:81.

[140] Ji Y, Liu W, Zhang ZQ, Wang XD, Li BX, Wang XF, Liu XY, Liu BB, Feng SH. Heterostructural $MnO_2@NiS_2/Ni(OH)_2$ materials for high-performance pseudocapacitor electrodes. RSC Adv. 2017;7(70):44289.

[141] Wang M, Wang Y, Dou H, Wei G, Wang X. Enhanced rate capability of nanostructured three-dimensional graphene/Ni_3S_2 composite for supercapacitor electrode. Ceram Int. 2016;42(8):9858.

[142] Zou X, Sun Q, Zhang YX, Li GD, Liu YP, Wu YY, Lan Y, Zou XX. Ultrafast surface modification of Ni_3S_2 nanosheet arrays with Ni-Mn bimetallic hydroxides for high-performance supercapacitors. Sci Rep. 2018;8(1):4478.

[143] Li YH, Shi M, Wang L, Wang MR, Li J, Cui HT. Tailoring synthesis of Ni_3S_2 nanosheets with high electrochemical performance by electrodeposition. Adv Powder Technol. 2018; 29(5):1092.

[144] Chen C, Zhou JJ, Li YL, Li Q, Chen HM, Tao K, Han L. $NiCo_2S_4@Ni_3S_2$ hybrid nanoarray on Ni foam for high-performance supercapacitors. New J Chem. 2019;43(19):7344.

[145] Wen J, Li SZ, Zhou K, Song ZC, Li B, Chen Z, Chen T, Guo YX, Fang GJ. Flexible coaxial-type fiber solid-state asymmetrical supercapacitor based on Ni_3S_2 nanorod array and pen ink electrodes. J Power Sources. 2016;324:325.

[146] Xiong X, Zhao B, Ding D, Chen DC, Yang CH, Lei Y, Liu ML. One-step synthesis of architectural Ni_3S_2 nanosheet-on-nanorods array for use as high-performance electrodes for supercapacitors. NPG Asia Mater. 2016;8(8):e300.

[147] Krishnamoorthy K, Veerasubramani GK, Radhakrishnan S, Kim SJ. One pot hydrothermal growth of hierarchical nanostructured Ni_3S_2 on Ni foam for supercapacitor application. Chem Eng J. 2014;251:116.

[148] Chou SW, Lin JY. Cathodic deposition of flaky nickel sulfide nanostructure as an electroactive material for high-performance supercapacitors. J Electrochem Soc. 2013;160(4):D178.

[149] Huo HH, Zhao YQ, Xu CL. 3D Ni_3S_2 nanosheet arrays supported on Ni foam for high-performance supercapacitor and non-enzymatic glucose detection. J Mater Chem A. 2014; 2(36):15111.

[150] Chou SW, Lin JY. Pulse-reversal deposition of nickel sulfide thin film as an efficient cathode material for hybrid supercapacitors. J Electrochem Soc. 2015;162(14):A2762.

[151] Li TT, Zuo YP, Lei XM, Li N, Liu J, Han HY. Regulating the oxidation degree of nickel foam: a smart strategy to controllably synthesize active Ni_3S_2 nanorod/nanowire arrays for high-performance supercapacitors. J Mater Chem A. 2016; 4(21):8029.

[152] Dhaiveegan P, Hsu YK, Tsai YH, Hsieh CK, Lin JY. Pulse-reversal deposition of Ni_3S_2 thin films on carbon fiber cloths for supercapacitors. Surf Coat Technol. 2018;350:1003.

[153] Niu SF, Zheng JH. $Mo_2S_3@Ni_3S_2$ nanowries on nickel foam as a highly-stable supercapacitor material. J Alloys Compd. 2018; 737:809.

[154] Zhong XW, Zhang LF, Tang J, Chai JW, Xu JC, Cao LJ, Yang MY, Yang M, Kong WG, Wang SJ, Cheng H, Lu ZG, Cheng C, Xu BM, Pan H. Efficient coupling of a hierarchical $V_2O_5@Ni_3S_2$ hybrid nanoarray for pseudocapacitors and hydrogen production. J Mater Chem A. 2017;5(34):17954.

[155] Han T, Jiang LY, Jiu HF, Chang JX. Hydrothermal synthesis of the clustered network-like $Ni_3S_2-Co_9S_8$ with enhanced electrochemical behavior for supercapacitor electrode. J Phys Chem Solids. 2017;110:1.

[156] Zhang JF, Lin JM, Wu JH, Xu R, Lai M, Gong C, Chen X, Zhou P. Excellent electrochemical performance hierarchical $Co_3O_4@Ni_3S_2$ core/shell nanowire arrays for asymmetric supercapacitors. Electrochim Acta. 2016;207:87.

[157] He WD, Wang CG, Li HQ, Deng XL, Xu XJ, Zhai TY. Ultrathin and porous $Ni_3S_2/CoNi_2S_4$ 3D-network structure for superhigh energy density asymmetric supercapacitors. Adv Energy Mater. 2017;7(21):1700983.

[158] Liu B, Kong DZ, Huang ZX, Mo RW, Wang Y, Han ZJ, Cheng CW, Yang HY. Three-dimensional hierarchical $NiCo_2O_4$ nanowire@Ni_3S_2 nanosheet core/shell arrays for flexible asymmetric supercapacitors. Nanoscale. 2016;8(20):10686.

[159] Long B, Balogun MS, Luo L, Qiu WT, Luo Y, Song SQ, Tong YX. Phase boundary derived pseudocapacitance enhanced nickel-based composites for electrochemical energy storage devices. Adv Energy Mater. 2018;8(5):1701681.

[160] Li LQ, Yang HB, Yang J, Zhang LP, Miao JW, Zhang YF, Sun CC, Huang W, Dong XC, Liu B. Hierarchical carbon@Ni_3S_2@MoS_2 double core-shell nanorods for high-performance supercapacitors. J Mater Chem A. 2016;4(4):1319.

[161] Zhou WJ, Cao XH, Zeng ZY, Shi WH, Zhu YY, Yan QY, Liu H, Wang JY, Zhang H. One-step synthesis of Ni_3S_2 nanorod@$Ni(OH)_2$ nanosheet core–shell nanostructures on a three-dimensional graphene network for high-performance supercapacitors. Energy Environ Sci. 2013;6(7):2216.

[162] Ji FZ, Jiang D, Chen XM, Pan XX, Kuang LP, Zhang Y, Alameh K, Ding BF. Simple in situ growth of layered Ni_3S_2 thin film electrode for the development of high-performance supercapacitors. Appl Surf Sci. 2017;399:432.

[163] Cheng LL, Hu YY, Ling L, Qiao DD, Cui SC, Jiao Z. One-step controlled synthesis of hierarchical hollow $Ni_3S_2/NiS@Ni_3S_4$ core/shell submicrospheres for high-performance supercapacitors. Electrochim Acta. 2018;283:664.

[164] Zhang Y, Sun WP, Rui XH, Li HT, Guo GL, Madhavi S, Zong Y, Yan QY. One-pot synthesis of tunable crystalline $Ni_3S_4@$amorphous MoS_2 core/shell nanospheres for high-performance supercapacitors. Small. 2015;11(30):3694.

[165] Wang LN, Liu JJ, Zhang LL, Dai BS, Xu M, Ji MW, Zhao XS, Cao CH, Zhang JT, Zhu H. Rigid three-dimensional Ni_3S_4 nanosheet frames: controlled synthesis and their enhanced electrochemical performance. RSC Adv. 2015;5(11):8422.

[166] Huang F, Sui YW, Wei FX, Qi JQ, Meng QK, He YZ. Ni_3S_4 supported on carbon cloth for high-performance flexible all-solid-state asymmetric supercapacitors. J Mater Sci: Mater Electron. 2018;29(3):2525.

[167] Duan XC, Xu JT, Wei ZX, Ma JM, Guo SJ, Liu HK, Dou SX. Atomically thin transition-metal dichalcogenides for electrocatalysis and energy storage. Small Methods. 2017;1(11):1700156.

[168] Huang JD, Wei ZX, Liao JJ, Ni W, Wang CY, Ma JM. Molybdenum and tungsten chalcogenides for lithium/sodium-ion batteries: beyond MoS_2. J Energy Chem. 2019;33:100.

[169] Wei ZX, Wang L, Zhuo M, Ni W, Wang HX, Ma JM. Layered tin sulfide and selenide anode materials for Li- and Na-ion batteries. J Mater Chem A. 2018;6(26):12185.

[170] Xue XG, Penn RL, Leite ER, Huang F, Lin Z. Crystal growth by oriented attachment: kinetic models and control factors. CrystEngComm. 2014;16(8):1419.

[171] Gou JX, Xie SL, Yang ZC, Liu YQ, Chen YJ, Liu YR, Liu CG. A high-performance supercapacitor electrode material based on NiS/Ni_3S_4 composite. Electrochim Acta. 2017;229:299.

[172] Zhang Q, Peng G, Mwizerwa JP, Wan HL, Cai LT, Xu XX, Yao XY. Nickel sulfide anchored carbon nanotubes for all-solid-state lithium batteries with enhanced rate capability and cycling stability. J Mater Chem A. 2018;6(25):12098.

[173] Tomiyasu H, Shikata H, Takao K, Asanuma N, Taruta S, Park YY. An aqueous electrolyte of the widest potential window and its superior capability for capacitors. Sci Rep. 2017;7(1):45048.

[174] Baptista JM, Sagu JS, Kg UW, Lobato K. State-of-the-art materials for high power and high energy supercapacitors: performance metrics and obstacles for the transition from lab to industrial scale—a critical approach. Chem Eng J. 2019;374:1153.

Qing-Hong Wang is a lecture in Jiangsu Normal University, China. She received her B.Sc. degree in Chemistry from Qufu Normal University in 2007 and her Ph.D. degree in Materials Physics and Chemistry from Nankai University in 2012. Between 2015 and 2016, she conducted the research at University of Wollongong as a visiting scholar. Her research focuses on the design and application of nanomaterials for energy storage and conversion, including rechargeable batteries and supercapacitors.

Wei Ni received his B.E. in Polymer Materials Science and Engineering from Zhengzhou University in 2005, and Ph.D. in Chemistry from Institute of Chemistry, Chinese Academy of Sciences (ICCAS) in 2011. After postdoc research fellow experiences including at Nanyang Technological University (NTU), Singapore, and University of Oulu, Finland, he is now a research staff at Panzhihua University and an adjunct research scientist at Chengdu University. His research interests include advanced nanomaterials for energy storage and environmental protection.

Jian-Min Ma is an associate professor in the Hunan University, Changsha, China. He serves as the Academic Editor for Rare Metals, and editorial board members for Journal of Energy Chemistry, Chinese Chemical Letters, Nano-Micro Letters, Journal of Physics: Condensed Matter, and others. His research interest focuses on the energy storage devices and components including metal anodes and electrolytes, and theoretical calculations from Density Functional Theory and Molecular Dynamics to Finite Element Analysis. He has published over 200 peer-reviewed papers.